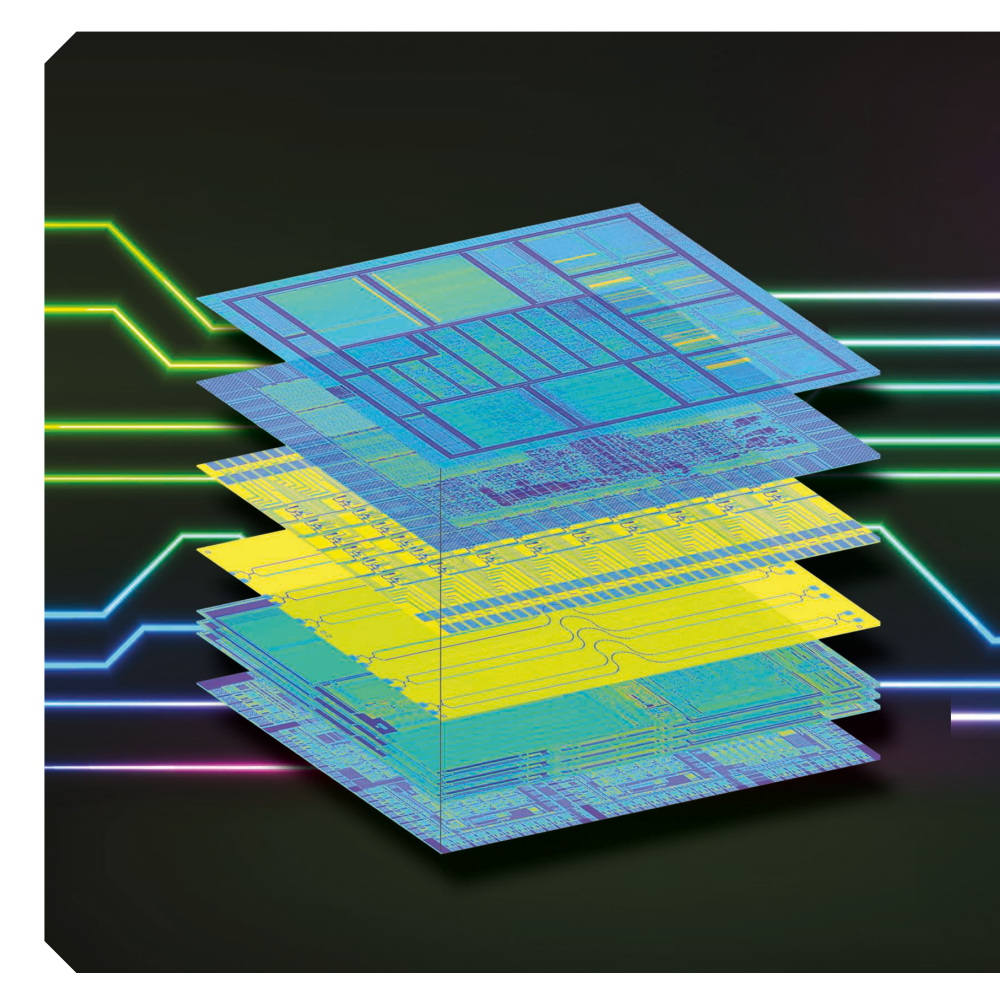
Toward 3D Integrated Photonics Including Lithium Niobate Thin Films

LITHIUM NIOBATE (LN) WAS THE dominant material platform for integrated optics for several decades, based on its superior electro-optical and nonlinear (NL) optical properties. However, silicon photonics, despite its less favorable intrinsic properties, has been rapidly adopted by industry to support a smaller device footprint; higher component density; lower energy consumption; and compatibility with high-volume, low-cost silicon microelectronics manufacturing processes. However, the performance of LN integrated optics remains unsurpassed by silicon photonics. By adopting a thin-film technology and hybrid waveguide designs, LN and silicon photonics could both be integrated as optoelectronics layers in future 3D integrated microsystems. We discuss the multilayer device architecture vision and recently reported enabling research progress in thin-film LN technology and its integration into the silicon photonics system.

THE CASE FOR INTEGRATING 3D AND HYBRID PHOTONICS

Today's state-of-the-art integrated microsystems inherited the design tools and

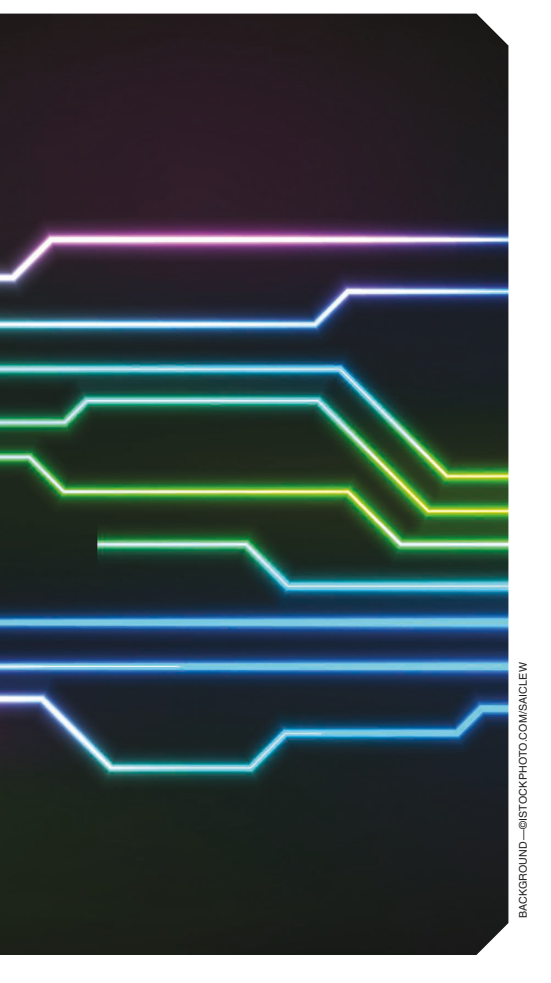


A bridge between electronics, radio frequency, and optical technology.

MICHAEL RÜSING. PETER O. WEIGEL. JIE ZHAO. AND SHAYAN MOOKHERJEA

Digital Object Identifier 10.1109/MNANO.2019.2916115
Date of publication: 10 June 2019

fabrication technology that was developed for digital processors and logic CMOS circuits in the past. However, they now incorporate a wide variety of other functionalities, including analog and mixedsignal electronics, radio-frequency (RF) and millimeter-wave (mm-wave) antennas, filters, mixers and amplifiers, accelerometers, transducers, microfluidic channels and valves, and light sources and photodetectors. Scalable and cost-effective wafer-scale manufacturing still is primarily a 2D technology. Thus, a complex, 3D



microchip-scale system can be realized by adopting a layered design and fabrication methodology and using interlayer connections between different modalities, as shown in Figure 1 [1].

Optics has an increasingly important role in current and future device technologies. In general, future large-volume applications of microchips include a global communications infrastructure

that spans and links hand-held devices, warehouse-sized computers, Internet of Things devices, medical and diagnostic systems, industrial automated monitoring applications, autonomous vehicular transportation and navigation systems (ground based, airborne, and space), and consumer electronics (virtual reality, telepresence, and entertainment). These are all areas in which one (or, in fact, more than one) optical layer in a 3D stack can improve functionality and performance.

Integrated optics can lead to the reduced size, weight, and power consumption of high-speed signal acquisition, quantization, and processing instruments, as well as improvements in interconnection technology and reduced susceptibility to electromagnetic. However, it is unlikely that a single optical material, or even a single optical layer, can meet all of the needs of today's complex microsystems. For example, integrated optical systems can improve the performance of state-ofthe-art clocks and frequency synthesizers [2], and of sensors and spectrometers [3], but they require many different integrated functions. Modern integrated optics can perform certain especially challenging tasks in machine intelligence [4], [5], quantum computing [6], and neuroscience [7], which require new operating modalities for optoelectronic devices.

In the not-too-distant past, LN was the standard platform of choice for complex photonic circuits and devices [8]. Although certain other materials, such as ceramics and polymers, may have higher intrinsic electro- and NL-optical coefficients, LN devices were fabricated with a high yield and were reliable in deployed operations. Today, (bulk) LN continues to be the state of the art for certain standalone devices, such as electro-optic modulators (EOMs), NL frequency converters, and quantum optics.

Recently, 3D structure fabrication in LN was performed using serial-write femtosecond laser patterning [9]. However, an alternative approach to 3D (or at least 2.5D) integrated circuits is possible, based on thin-film technology and hybrid waveguides. We recognize that Si photonics, rather than LN photonics, has rapidly scaled up in the last two decades by leveraging the manufacturing technology and

wafer-scale processing toolsets that the microelectronics industry developed and refined [10]-[14].

Table 1 summarizes the basic parameters of the integrated optics materials bulk and thin-film LN and silicon, as well as III-V semiconductors, which play an increasing role as active laser and gain material in the silicon photonics environment [15]. The values are intended to provide an indication of the typical values observed in many realized devices. Depending on the waveguide geometry and confinement method, the values may show a dependence on the light polarization. Due to mutual dependencies between certain properties in single instances, different values can be reached. However, it is often at the cost of another parameter, e.g., a high confinement might lead to increased propagation loss due to the increased influence of surface roughness or the lowest useful confinement is limited by NL loss effects, e.g., two-photon absorption, for a given power.

A stack-integration approach would allow engineers to harness the remarkable optical properties of this multifunctional material within the maturing Si photonics ecosystem of scalable design and foundrybased fabrication process flow. This article discusses various optical devices that the hybrid materials platform can form. In addition, the proximity to silicon layers and driver circuits would be a substantial and obvious benefit for monitoring, bias-point tuning, and low-parasitic driver integration, which future integrated microsystems will most certainly require.

THIN-FILM LN: AN INTEGRATION STRATEGY AND OPTICAL **WAVEGUIDES**

LN has been used since the early days of integrated optics. It offers a remarkable combination: a wide electromagnetic transparency window over RF wavelengths from near-dc to terahertz and optical wavelengths from about 400 nm to 4.5 µm, over which it exhibits significant NL and electro-optic constants. LN also has pyroelectric, piezoelectric, and ferroelectric properties, can be grown in large single crystals (75-150 mm in diameter), and is a good conductor of heat [41], [42]. Along with a mature bulk-LN optical device technology that has already been applied in deployed communication networks and systems, there has been a multidecade effort to fabricate thin films by deposition and epitaxy, but many initial efforts were of poor optical quality [43].

While there is still considerable progress to grow optical-quality LN epitaxially

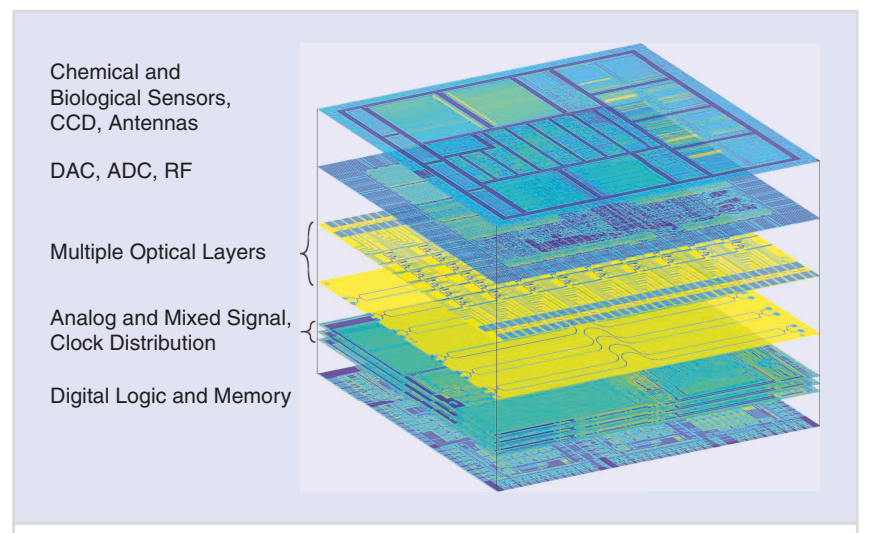


FIGURE 1 The vision of 3D integrated microsystems. (Modified from Peter John Bishop, Angeloleithold, and Antoine Bercovici.) ADC: analog—digital converter; DAC: digital—analog converter.

[44], thin films now are commercially fabricated quite reliably with an ion-slicing and wafer-bonding technique known as crystal ion slicing [45]. This process fabricates LN thin films with material properties similar to those of bulk LN [46], of thicknesses down to a few thousand angstroms bonded to a buffer layer, i.e., silicon dioxide, on the handle material. Vendors can commercially procure this crystalline thin-film material, known as lithium-niobate-on-insulator (LNOI), on 3- and 4-in wafers. LNOI is available in various crystal cuts, at different thicknesses, with or without dopants (e.g., MgO for high optical power applications), with buried electrodes, and on various handles (e.g., Si or LN). Similar to LNOI, isostructural lithium tantalate (LT) also is available in the form of single crystalline thin films on an insulator from commercial sources [47]. In general, LT offers properties similar to LN, but the different absolute values of the material constants,

Į,	TABLE 1	An overview of the typical material and technical properties observed for the integrated optics platforms bulk LN, LNOI,
ľ		silicon photonics, and III-V semiconductors.

PLATFORM	BULK LN	LNOI	SILICON PHOTONICS	III-V PHOTONIC CIRCUITS
Optical loss (1,550 nm)	0.02-1 dB/cm [16], [17]	0.03-3 dB/cm [18], [19]	1–3 dB/cm [20], [21]	1-4 dB/cm [22]
Mode cross section	5–25 μ m 2 [23]	$\approx 1 \mu \text{m}^2$	$< 1 \mu \mathrm{m}^2$	$<$ 1–5 μ m 2 [24], [25]
Confinement (method)	Δn < 0.1 (diffusion) [17]	$\Delta n = 0.7 \text{ (SiO}_2/\text{LN) [23]}$	$\Delta n = 2.0 \text{ (SiO}_2/\text{Si)}$	$\Delta n \approx 0.1-0.4$ (heterostructures); $\Delta n > 2$ (GaAs-oninsulator) [23], [25]
Bending radius	$>$ 500 μ m [26]	$<$ 10 μ m [27], [28]	$<$ 10 μ m	<100 µm [22]
Wafer diameters	75–150 mm	75–100 mm	200-300 mm	100-200 mm
Leveraging industry and technologies	RF industry (SAW and BAW filters)	Silicon CMOS (ion- slicing, bonding, and CMP); bulk-LN technology	Silicon CMOS	HBTs and lasers
Photonic-electronic integration	RF to optics (acousto- optic and electro-optic)	RF to optics (acousto- optic and electro-optic)	Silicon CMOS (detectors, P–N junctions, and electronics)	Laser diodes and detectors
Optical gain and light sources	Limited gain (e.g., Erdoping) [29]	Limited gain (e.g., Er- doping) [30]	No efficient gain or lasers; recent hybrid III-V integration [31], [32]	Efficient gain and lasers (electrically pumped) [31]
Optical modulation mechanisms	Pockels effect	Pockels effect	Carrier dispersion and plasmonics	Pockels effect, carrier dispersion, and Kerr effect
Electro-optical con- stant (Pockels effect)	Up to 33 pm/V (<i>r</i> ₃₃) [33]	Same as bulk	_	1–2 pm/V (AIN, InP, and GaAs) [34], [35]
NL optical effects	$\chi^{\scriptscriptstyle (2)}$ (SHG, PDC,); $\chi^{\scriptscriptstyle (3)}$	$\chi^{\scriptscriptstyle (2)}$ (SHG, PDC,); $\chi^{\scriptscriptstyle (3)}$	$\chi^{\scriptscriptstyle{(3)}}$ (FWM,)	$\chi^{ ext{ iny (2)}}$ (SHG, PDC), $\chi^{ ext{ iny (3)}}$
$oldsymbol{\chi}^{ ext{ ext{ ext{ ext{ ext{ ext{ ext{ ext$	Up to $d_{33} = 27 \text{ pm/V}$ [27]	Same as bulk	_	1 pm/V (AIN), up to 119 pm/V (GaAs) [35], [39]

FWM: four-wave mixing; HBT: heterojunction bipolar transistor; AIN: aluminum nitride; PDC: parametric down conversion.

e.g., pyro-electricity [47] or birefringence [48], may be advantageous for specific applications.

Optical waveguides fabricated in bulk LN are typically realized by physically or chemically altering the refractive index of the material [49]-[52]. In principle, in thin-film LN optical devices, waveguides can be formed by similar methods in bulk, such as proton exchange (PE) [53] and titanium in-diffusion [17]. Titanium indiffusion requires temperatures greater than 1,000 °C, which could damage the bonding interface of LNOI films [54]. In addition, waveguiding can be achieved by generating crystal damage (and, thus, a refractive index change) in certain regions through ion implantation or direct laser writing [55], [56]. Waveguides defined in bulk LN show low propagation loss (about 0.02 dB/cm [16] at a wavelength of 1.32 μ m). Similarly, for PE thin-film waveguides, losses down to 0.2 dB/cm have already been reported [26]. The PE process only enhances the extraordinary index, i.e., along the z-axis [17]. Therefore, PE-exchanged waveguides only support one polarization, depending on the crystal cut that was used [26].

Because the core-to-cladding refractive index contrast (typically $\triangle n \approx 0.1$) in bulk-LN waveguides is small, the optical waveguide bending radius is large. In fact, the most complex bulk-LN photonic circuits often have only approximately 10 elements/cm² [57]. This means that traditional LN waveguide fabrication methods may not be the best candidates to define compact optical structures within a layer-stacking approach, despite providing μm^2 confinement bending radii that are greater than 500 μ m [26].

To overcome this challenge, a stronger form of horizontal optical mode confinement is helpful and potentially offers an order-of-magnitude smaller mode volumes and tighter bend radii compared to bulk LN very similar to silicon photonics, as shown in Figure 2. Two methods are gaining prominence: the thin film of LN can either be etched into a waveguide [28], [58]-[61] and surrounded by a low-index cladding material, such as silicon dioxide [62], or it can be ridge-loaded by a patterned strip of a second material, such as silicon or silicon nitride, and then surrounded by the cladding. Figure 3 shows examples for various waveguides realized in LNOI.

Regarding the first method (etching), ribs and ridges in thin-film LN have been fabricated using wet and dry etching [62], Ar milling [63], and a cutting tool like a diamond blade [19]. When the sidewall roughness is controlled, favorable low losses down to 0.03 dB/cm can be achieved [64], [65]. This is similar to losses in bulk-LN waveguides and is lower than typical values of 1-3 dB/cm for Si photonics [20].

The second method (ridge loading) requires a second waveguiding material in addition to LN itself, whose refractive index is higher than that of the cladding (SiO₂). Various materials that have been deposited are TiO2 [66], Ta2O5 [23], Si₃N₄ [67], chalcogenide glass [68], or (amorphous) silicon [33], [69]. Optical mode areas as small as $1 \mu m^2$ are possible

[69]. The strip-loading waveguides are often thin (<300 nm) to achieve a large optical-mode overlap with the LN region. Reducing the strip surface roughness and thickness variations can lower the optical propagation losses [70].

Deposited ridge-loading materials are usually amorphous or polycrystalline, which have a higher optical propagation loss, poor electrical and thermal conduction properties, and uncertain aging behavior compared to their crystalline counterparts. If the bonded stack already incorporates diodes or transistors, or would be affected by built-up strain or stress, it may not be possible to use a hightemperature annealing process to convert the amorphous material into a crystalline format without impacting the rest of the stack. Therefore, bonding is a potentially useful technique to integrate thin-film LN into a multilayer stack [71], following the approach already used to integrate III-V semiconductors onto silicon photonics.

Typically, III-V to Si waferbonding is done in the following steps: 1) pattern a silicon-on-insulator (SOI) wafer with features required for waveguides, modulators, and (usually) detectors; 2) chemicalmechanical polishing (CMP) of surfaces on both wafers; 3) the bond select die cuts from a III-V wafer to the SOI wafer; and 4) pattern the combined stack (if necessary). In this a so-called hybrid device, two or more material layers share the optical mode and transitions are made with lithographically defined structures (singlelayer or bilayer tapers or gratings integrated into waveguides).

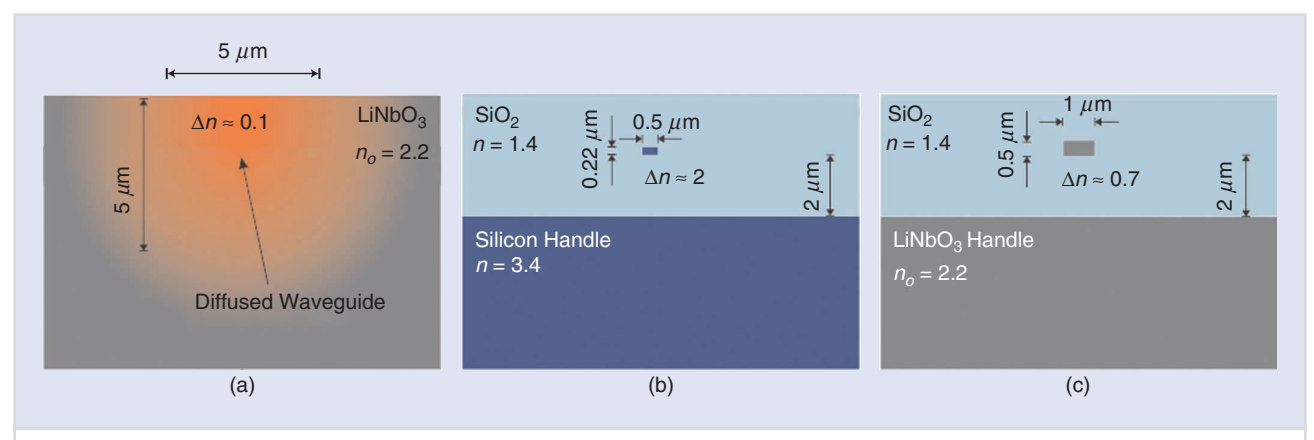


FIGURE 2 Cross sections (to scale) of typical waveguiding structures. (a) Bulk lithium niobate, (b) silicon-on-insultator, and (c) lithium niobate on insulator.

In a similar spirit, our recent research has shown integrated crystalline thin-film LN with crystalline silicon [27], [72], with both layer thicknesses in the few thousand angstrom regime. Silicon-loaded LN hybrid waveguides have a higher effective modal refractive index, and thus permit smaller-radius bends and denser integration than etched LN waveguides. Although the technical details are important and vary between published reports, [40], [54], and [73]-[75] describe a fabrication approach that is similar in principle.

In our work, the features required for optical waveguiding were defined using photolithography and etched on an SOI wafer (150-nm Si thickness, 3-um oxide thickness), whereas the LN wafer was left unpatterned and unetched. The thin (<50-nm) oxide separation that exists between Si and LN after bonding was defined by an oxide deposition, CMP, and oxide-thinning process. 600-nm x-cut LN films were commercially procured (NanoLN, Jinan Jingzheng Electronics) in the form of a 75-mm wafer separated from a Si handle by a 2-µm layer of SiO₂. SOI and LNOI wafers were diced and individual dies were cleaned using an RCA-1 wet etch. The plasma surface activation of both the SOI and LNOI dies was achieved with a microwave frequency plasma asher at 150 W and 1.1 mbar for 150 s. The dies were immediately placed in deionized water for 10 min and then pairs of SOI and LNOI dies were dried with nitrogen gas and bonded at room temperature. Bonded samples were annealed under pressure, using a modest heating cycle (200 °C for 1 h followed by 250 °C for 1 h, 300 °C for 2 h, and natural cooling back to room temperature), which should not deteriorate the diodes and transistors defined in the silicon layer.

The bonded stack has been shown to withstand repeated temperature cycling to at least 300 °C [76], which is sufficient for the postprocessing that we required here. In our work, the same chips were repeatedly processed after bonding, through multiple cycles of electrode formation, removal, and reformation, searching for the optimal device dimensions, without apparent degradation. Following bonding, the handle on the LNOI side (which is Si) was removed with an XeF2 isotropic dry etch. Before the XeF2 etch, all other areas of the bonded sample were coated with a protective layer of temporary bonding material (BrewerBond 220, Brewer Science) to prevent undesired etching of the SOI substrate and waveguiding features. The 2-µm SiO2 insulator was removed with a hydrofluoric acid-based wet etch.

To form electrodes, aluminum was deposited on the LN thin film by sputtering. (Gold is another, although costlier, choice.) A 10-nm chromium adhesion layer and RF coplanar waveguide structures when needed (e.g., for modulators) were patterned using photolithography. Since LN is a transparent material, alignment markers patterned on the Si layer make the aligned-lithography process relatively simple. The smaller size of commercially available LNOI wafers (75-mm diameter) compared to the much larger silicon wafers suggests a die-bonding strategy, rather than a wafer-bonding approach, at present. (Also, die bonding is less costly when researching and developing on the fabrication process.) Transferring this fabrication process to wafer scale has not yet been performed. The CMP process used in our research has unoptimized uniformity across the wafer [72] and we expect significant improvements through process iterations.

Most of the fabricated waveguide structures in thin-film LN can provide single-mode operation of um confinement. An example of multimode operation was shown for wide-diced [19], [30] or etched waveguides [28] and may be preferred for certain applications, e.g., in the NL frequency conversion as discussed below. Due to the slab geometry of thin-film LN, many demonstrated waveguides feature a high vertical confinement but a lower horizontal confinement. Therefore, by design, the transverse electric (TE) mode features the higher effective index and often a slightly lower loss than the lowest order transverse magnetic (TM) [19], [28], [66]. The intrinsic birefringence of LN can, however, cause the lowest TM mode featuring a higher index for certain designs

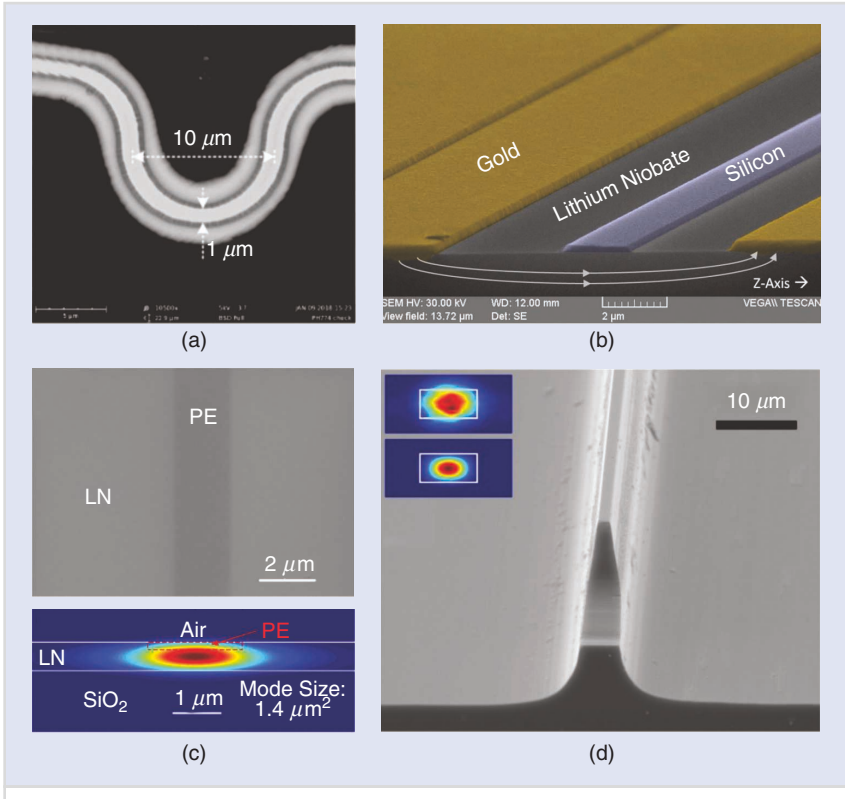


FIGURE 3 Scanning electron microscope (SEM) micrographs of different waveguide types realized in LNOI. (a) The top view of an etched waveguide demonstrates a small bend [28]. (b) Cross-sections of a strip-loaded silicon waveguide with gold electrodes form a phase shifter [40]. (c) The top view of a PE waveguide and the calculated mode profile [26]. (d) The coupling facet of a diamond blade diced waveguide. The insets show the measured (top) versus calculated mode profile [19]. (Source: The Optical Society; reprinted with permission.)

and geometries despite the wide aspect ratio of the waveguide, e.g., in hybrid silicon thin-film LN waveguides [27].

INTEGRATED PHOTONICS COMPONENTS USING THIN-FILM LN

In a multilayer stack, waveguides can be defined in each of the separate optical layers without crosstalk or in combinations of layers (which are called hybrid waveguides). Accordingly, we separate our discussion of thin-film LN-based devices into single-layer and bilayer structures. We can expect to see trilayer and multilayer structures in the near future, since they have been introduced relatively recently in conventional silicon photonics [77], [78]. Die stacking with even more optical layers remains a subject of future research.

This section discusses the main issues and challenges in single-layer and multilayer optical structures using thin-film LN, some examples of which Figure 4 shows. We do not discuss electrical (lowfrequency) signal interconnections, since vertical electrical interconnects and multilayer metal traces are a standard part of existing CMOS-compatible foundry processes. We also do not explore RF and mm-wave electrical signal propagation, confinement, and crosstalk issues in the die-stacking picture, which are important but require careful consideration in their own right.

SINGLE-LAYER BUILDING BLOCKS

Photonic circuits are built from waveguides, directional couplers, and inputoutput couplers. Simple directional coupling between two waveguides close to each other occurs through their evanescent tails; the effect is fairly strong and nearly full-power coupling can be achieved in less than 10 µm. Thus, directional couplers in LNOI devices have existed since the earliest reports of integrated devices, such as between a resonator and a bus waveguide [73].

An alternative form of coupler is the multimode interference (MMI) coupler structure [83], [84], which can be more fabrication tolerant or offer broadband operation. Li et al., for example, designed and demonstrated a 1×2 and a 2×2 MMI as splitter and combiner, respectively, of an asymmetric Mach-Zehnder interferometer (MZI). The entire

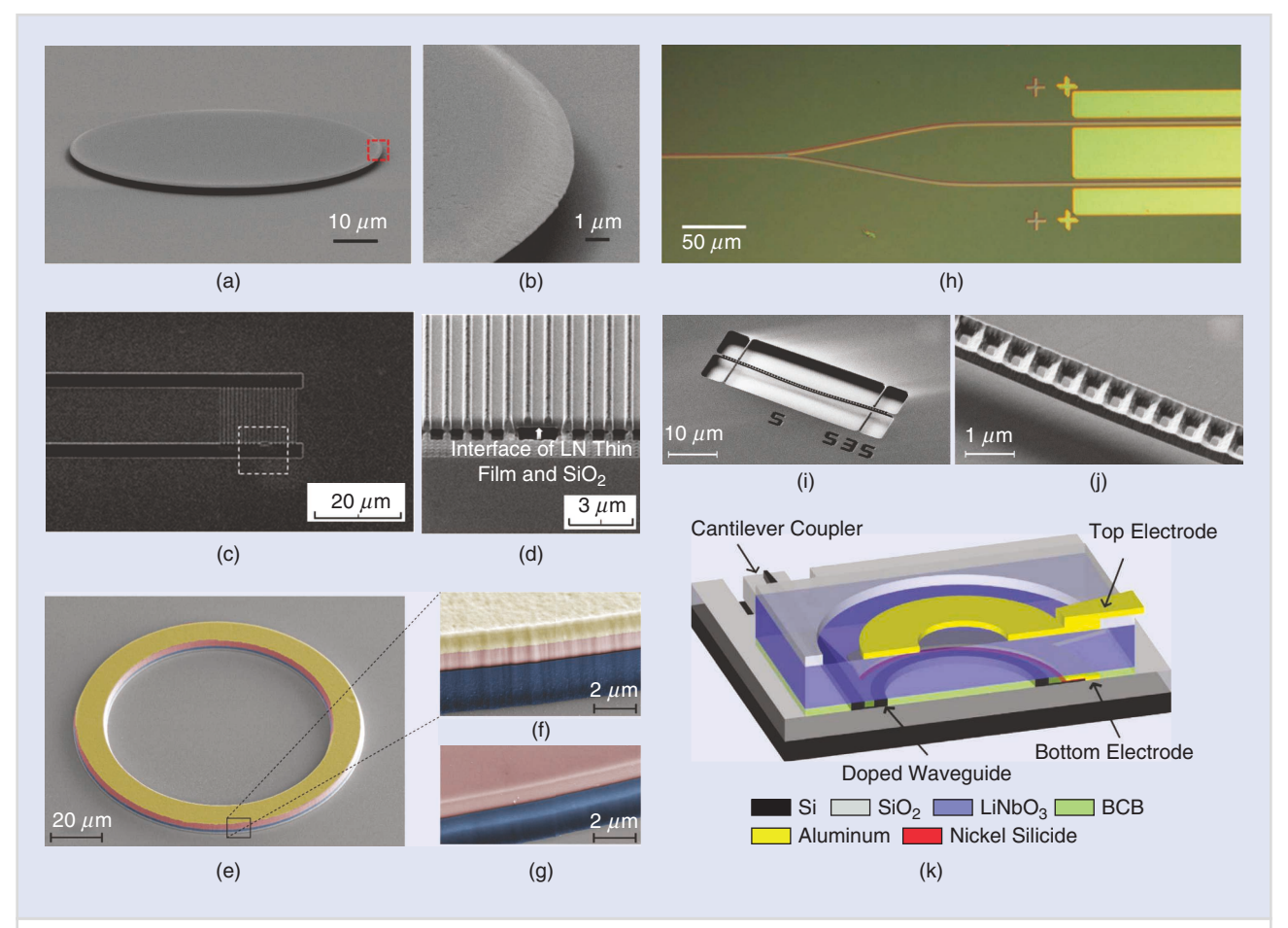


FIGURE 4 (a) and (b) SEM micrograph and closeup of a disk resonator fabricated in thin-film LN. Resonators in thin-film LN with Q > 10⁶ have been demonstrated [64], [79]. (c) and (d) An SEM micrograph of an etched LN waveguide and grating coupler and closeup of the grating [80]. (e)-(g) A false color SEM micrograph of an etched LN microring and closeup of the side wall before (f) and after (g) polishing. The silicon dioxide is colored blue and the lithium niobate is colored red and yellow, which shows the chromium layer protecting the LN during polishing [81]. (h) An optical micrograph of a y-junction leading to a modulator section formed by an amorphous silicon strip-loaded waveguide [40]. (i) –(j) SEM micrographs of etched photonic crystal nanobeam resonators. The photonic crystal resonators feature a very favorable Q-factor to mode volume Q/V ratio [82]. (k) A schematic of a hybrid silicon LN microring electro-optic tunable resonator [73]. (Source: The Optical Society; reprinted with permission.)

interferometer operated from 1,530 to 1,610 nm with negligible polarization dependence, but no specific performance on the single-MMI operation was presented [83]. Merging two waveguides forms a Y-junction [26] that is similar to a 2×2 directional coupler in which the higher-order mode in the combined region is typically lost to radiation.

For large networks of couplers (used in cross-bar switches or optical simulator studies), Y-junctions can offer cleaner transmission spectra compared to standard directional couplers but the challenge is to minimize the excess loss in the coupling region (beyond 3 dB). Y-junctions in LNOI have, for example, shown PE waveguides or strip-loaded amorphoussilicon waveguides serving as the combiner and splitter in an MZI. The PE waveguide designs show a 0.24-dB total insertion loss for the splitter, but the design was considerably large compared to other LNOI designs (length $> 500 \mu m$) and showed only a single polarization operation due to the PE waveguide [26].

Resonators provide wavelength selectivity and add/drop functionality, which are needed in optical communications and switching, as well as optical intensity enhancement, which find uses in wavelength conversion and sensing applications. Among the simplest forms of resonator structures are microdisks, which are formed from a cylindrical region of thinfilm LN and support whispering-gallery optical modes [79].

By bending a waveguide onto itself, a microring resonator forms. Compared to microdisks, microring resonators are more selective in terms of the optical modes that can exist (as few as one transverse mode) and, thus, exhibit a cleaner transmission spectrum with a larger separation between the targeted resonance and undesired resonances that may exist at nearby wavelengths. Microring resonators with side-coupled bus waveguides were among the earliest types of optical devices fabricated in thin-film LN [85]. The bending radius has decreased from about $100 \, \mu \text{m}$ (low free spectral range) in the earlier works to about $10 \, \mu m$ due to improved lithography.

Electrodes have been incorporated for tuning the resonance wavelength, thus achieving optical filtering functionality. In earlier work, the quality factor of the resonance was low (10,000 or less) and tuning efficiency was also quite low (about 0.14 GHz/V [85]). This combination meant that high voltages were required for noticeable changes in transmission, which was previously observed in etched bulk-LN microring resonators (about 0.19 GHz/V) [86]. Recently, the performance of tunable ring filters has improved to 1.56 GHz/V [87] and other types of structures can also be used as electro-optically tunable wavelength interleavers [83]. A structure similar to the one used for a voltage-tuned optical filter can, naturally, be used as an EOM. An electrical modulation bandwidth as high as 7.5 GHz was achieved in the case of the x-cut LN film bonded to a Si racetrack resonator [88], [89]. These kinds of compact resonant electro-optic devices can have other interesting applications, including electro-optic comb generation and packet switching [90], [91].

Lately, microring resonators with a high quality factor $(Q > 10^6)$ [64] have been fabricated by reducing the sidewall roughness of etched thin-film LN waveguides with polishing. The microrings demonstrated in this article have a large radius of curvature (about 100 μ m) and our conjecture that, for radii below 40 μ m, the roughness-reduction scheme might not be effective. In addition, integrated directional couplers have not been demonstrated on this platform, making it difficult to achieve large extinction ratios and critical coupling. Nevertheless, strategies for improving the propagation loss of integrated LNOI structures are broadly useful for all potential applications.

Certain applications, such as light-matter coupling, benefit from enhancing not just the quality factor (Q) of the resonance, but also reducing the optical mode volume (V) as much as possible. Generally, the structures that support the highest Q/V ratios in other forms of integrated photonics are photonic crystals, which have been studied in thin-film LN as well [46]. Argon ion milling has been used to make 1D photonic crystal structures, followed by a dilute high-frequency (HF) undercut etch to suspend the waveguides (a nanobeam structure)

[82], [92]. Focused-ion beam (gallium) milling, followed by a dilute HF etch-away of the damaged layer near the surface, is another technique that has been explored to make 2D periodic arrays of holes in thin-film LN, which is required for photonic crystals, line-defect waveguides, and resonators [93]. Alternatively, the resonator pattern can be formed in silicon, before bonding to LN [75], and the better-controlled etching processes resulted in an experimentally achieved (loaded) Q-factor, $Q > 10^5$, which is substantially higher than in photonic crystals formed in LN. On the other hand, less than 20% of the energy of the resonant mode was contained in LN.

Polarizers [94] and polarization beam splitters (PBSs) [95] are another set of useful in-plane optical structures that have been realized in thin-film LN. So far, designs have only been theoretical, but the proposed polarizer based on shallow etched LNOI is expected to have a high extinction ratio of 108 dB/mm for TE pass and 27 dB/mm for TM pass [94], while the proposed PBSs in a ridge LNOI structure is expected to provide more than a 10-dB extinction ratio in a 65-nm broad operation around 1,550 nm with a maximum of up to a 35-dB extinction ratio. A full-scale polarization rotator and tracker has not yet been demonstrated in thin-film LN but, given the commercial availability of their bulk-LN counterparts, we can safely conjecture that their development is not far in the future.

Grating couplers [68], [80], [96] are a way to couple light from free-space optical beams and light launched from the end of a fiber into waveguides. To improve coupling efficiency beyond 50% (-3 dB), a bottom reflector made of a thin film of gold (between the LN and the silicon dioxide cladding layer in the LNOI wafer) may be used. The thickness of the oxide layer is also important, to maximize the coupling efficiency at a particular wavelength. While grating couplers can be optimized for a particular wavelength band (e.g., a range of wavelengths close to 1,550 nm), it is not known how to design a single grating coupler that is simultaneously efficient at very different wavelengths, e.g., for second-harmonic, sum-frequency, or

difference-frequency generation. However, the different wavelengths may be coupled in and out at different points of the optical circuit, if a common oxide thickness can be supported.

Gratings couplers in LNOI have been realized, such as by etching LNOI directly [80], [97], defined in amorphous silicon in a strip-loaded geometry [40] or chalcogenides [68]. In chalcogenide, an insertion loss of down to 6.2 dB was predicted for the TE polarization, while the fabricated device showed an approximately 10-dB insertion loss. For etched designs without a metal back-reflector, the experimentally achieved results for TE coupling are similar (9.1-dB insertion loss in the experiment versus a prediction of 3.2 dB). With a metal reflector, this was improved to a 6.9-dB insertion loss. The theoretical predictions show that values below 3 dB are in reach.

TWO-I AYER AND HYBRID **BUILDING BLOCKS**

When two or more optical layers are stacked on top of each other, optical devices may be designed in either or both layers, with vertical interlayer transitions, or in combinations of both layers, i.e., the optical mode is partially distributed between the two layers. The combination of planar lightwave circuits (PLCs) in silica-integrated optics and LN waveguide modulators to make a combined (though not vertically integrated) device was demonstrated more than a decade ago [98]. The input and output ports, as well as a coupler for monitoring, were realized in the silica PLC section, whereas the phase-shifter sections were fabricated on an LN substrate.

Integrating multiple optical layers requires vertical optical interconnections. These are quite common in silicon photonics, which includes a separate layer for germanium photodetectors, and for III-V semiconductor lasers and amplifiers. A variety of techniques exist for transitioning light between optical layers, including one or bilayer waveguide tapers [78], [99], [100], grating couplers [101], or etched reflectors (also known as optical proximity couplers [102]), as shown in Figure 5. Relatively recently, vertical optical interconnections have been designed for thin-film LN as well. For example, silicon- LN tapers are

discussed in [27] and silicon nitride-LN tapers are discussed in [67] and [103].

The interlayer-coupling scheme shown in Figure 5(a) relies on interactions between the evanescent tails of waveguide modes; therefore, the vertical gap h between the waveguides has to be quite small, especially in high index contrast platforms such as silicon photonics (a few hundred nanometers). For low-crosstalk waveguide-waveguide overpasses, an intermediate layer may be required [78]. Such couplers are generally governed by coupled-mode theory and grating structures may be included in the design to help with phase matching between differing modal effective indices if the two optical layers are composed of different materials. In certain embodiments, one

of the tapers can be left out if the other taper does not vanish all the way to zero width, but retains a certain minimum size [27], [72]. In contrast, the coupling schemes shown in Figure 5(b) and (c) rely on mode conversion between a confined waveguide mode and a radiating field pattern. They offer greater flexibility in design and layer distance and can be made more compactly, but generally do not have as many end-to-end coupling efficiencies as the scheme shown in Figure 5(a). These structures may require precise fabrication and additional processing steps to incorporate the backside mirrors, which improves the directional selectivity of the radiation in the preferred direction.

In [104], the input and output sections, as well as the directional couplers,

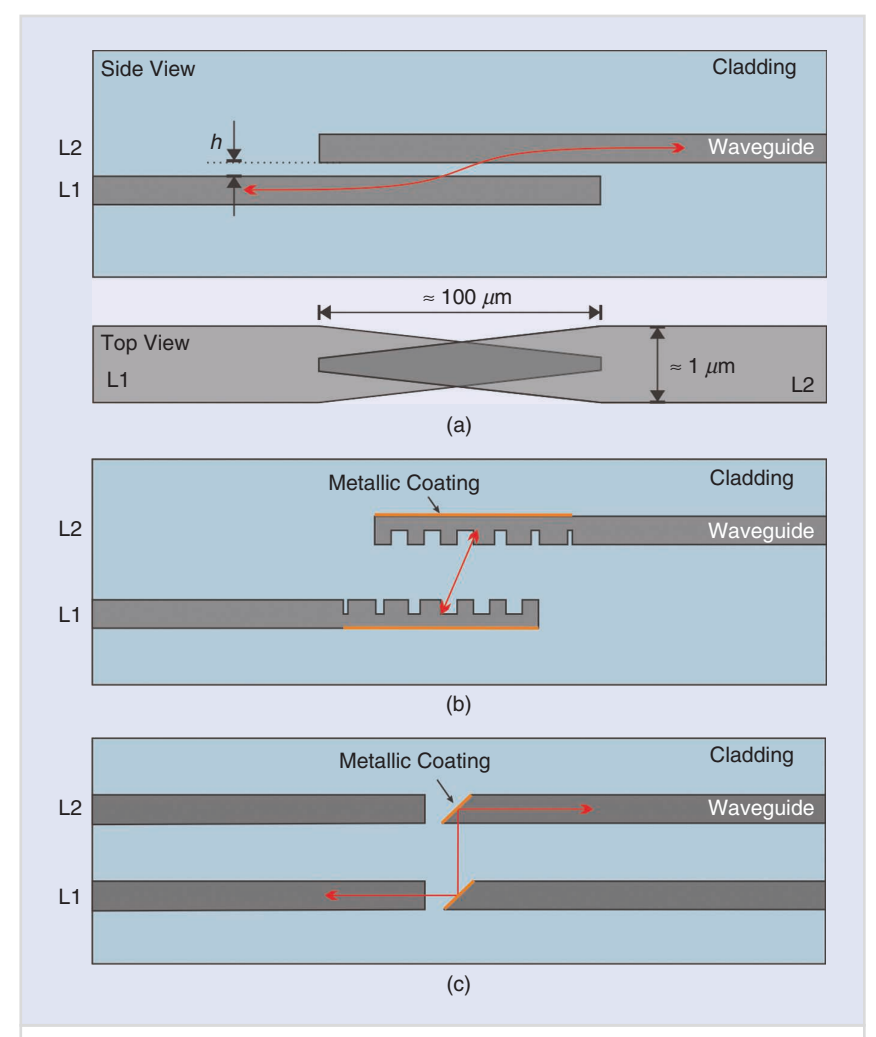


FIGURE 5 Examples for an interconnection between optical layers L1 and L2 (images not to scale). They are the same or different materials and are (a) waveguide tapers that rely on evanescent field coupling [78], [99], [100], (b) grating structures [101], or (c) optical proximity couplers [102].

were realized in single-mode silicon nanophotonic waveguides (with an oxide cladding) and the phase-shifter sections were realized in a hybrid mode that consisted of the bonded combination of thin-film LN and a narrow and thin Si rib feature, surrounded by oxide. The presence of the Si rib feature ensures that the optical mode is confined and localized without having to etch LN, which has traditionally been problematic [105] and, despite recent advances in etching quality, may not be compatible with CMOS foundry processing.

As shown in [27], hybrid modes can exist over a wide range of design parameter choices: from those that confine nearly all of the light energy in LN to those that guide light mainly in the other material. Some hybrid modes, especially the Si-LN modes, can achieve very tight optical bends (bending radii about 10 µm or less) under an unpatterned, unetched LN slab, which is not possible with conventional LN waveguides.

In the future, we expect to see trilayer (or even greater numbers of layers) hybrid waveguides, e.g., Si-Si₃N₄-LN structures, that can be useful for reducing edge transition loss and multiwavelength operation, as required in NL optics.

APPLICATIONS OF THIN-FILM **LN IN PHOTONICS**

The most common applications of LN in integrated optoelectronic devices are in EOMs and NL optical devices. In both cases, newly developed devices based on LN thin films appear to offer superior performance over traditional bulk-LN-based devices. Moreover, incorporating thin-film LN provides much-needed functionality into the silicon photonics ecosystem, as silicon itself possesses neither a strong and reliable second-order NL nor pure (i.e., loss-free) electro-optic properties that are comparable in magnitude to LN.

EOMs

EOMs serve the function of quickly switching an optical signal on or off, and are a critical component in modern fiber optic links. In recent years, Si absorption and phase modulators have been constructed based on the carrier dispersion effect. They can be included in foundry processes on a small footprint (down to a few micrometers, in the case of plasmonically assisted devices). Carrier-based modulators are limited by the tradeoffs between optical absorption and achievable phase change [31], and plasmonic modulators may suffer from mode transition losses when coupling to optical fibers or free space modes. In LN (and other similar crystals), Pockel's electro-optic effect provides a phase change without inherently increasing optical absorption because of the phase change. The low amplitudephase coupling effects, i.e., chirp, benefit the performance of high-bandwidth, longrange optical communication systems traveling through long lengths of dispersive optical fiber. Therefore, LN EOMs, particularly the MZI structures that do not have feedback (resonant) optical paths that can limit bandwidth, have been the gold standard of modulator device technology for several decades [106].

These aspects of the bulk-LN EOM still exist in the LN thin-film platform,

though additional benefits, such as reduced half-wave voltage-length product $(V_{\pi}L)$, increased photonic circuit density, and a smaller EOM footprint, are made possible by the 10-100-times reduction in the optical mode area [107], as shown in Table 2. The standard figure of merit for an MZI EOM is the product $V_{\pi}L$

$$V_{\pi}L \propto \frac{\lambda_0 G}{\Gamma_{mo}}$$
,

where V_{π} is the voltage required to shift the optical phase by π radians (corresponding to a switch between the on and off states in an intensity modulator), L is the length along which the voltage is applied, λ_0 is the free-space optical wavelength, G is the gap between ground and signal electrical lines, and Γ_{mo} is the normalized overlap between the optical and electrical fields over the LN region in the transverse plane. Due to their high index contrast, waveguides in LN thin films can be used to support modes an order of magnitude smaller than bulk-LN waveguide modes (see Figure 2), meaning that G—and thus $V_{\pi}L$ —can be reduced by nearly an order of magnitude without inducing unacceptable optical losses. A 10-times reduction in V_{π} results in 100-times less drive power, while a 10-times reduction in device length (L) can result in a wider modulation bandwidth [108], as well as a much smaller device footprint.

The electro-optic effect is described in terms of a second-rank tensor. As not all tensor elements are nonzero or of the same magnitude, the correct orientation of waveguide, light polarization, electrodes, and crystal is essential. The largest electro-optic tensor element, r_{33} , is observed for an interaction between light and the electric field, both polarized along the z-axis of the LN crystal [41]. So far, many devices have been designed to primarily support the TE mode. Hence, x-cut is the preferred crystal cut for many devices with waveguides oriented in the y direction.

Modulation of TM is possible, requiring either a different crystal cut, e.g., z-cut or addressing other tensor elements by different electrode geometries. For example, the device in Figure 4(k) uses z-cut LN, while the back-electrode is provided by the doped Si waveguide itself. This allows access to the r_{33} for TM polarization for optimal

	•			
PLATFORM	BULK LN	LNOI	III-V (InP)	SILICON PHOTONICS
Reference	[36]	[18]	[37]	[38]
Mechanism	Pockels effect	Pockels effect	Multiple effects	Carrier dispersion
V_{π}	3.5-5.1 V	1.4 V	2 V	0.5-7.6 V
Extinction ratio	20 dB	30 dB	25 dB	6.5-20 dB
Modulation bandwidth	70 GHz	Up to 100 GHz	Up to 54 GHz	10-50 GHz
Insertion loss	< 5.6 dB (including chip coupling)	< 0.5 dB	6 dB	1–12 dB
Energy per bit	< 300–900 fJ	0.37-14 fJ	517-2,510 fJ	50-30,000 fJ

performance, but modulation in TE is possible by using the smaller r_{13} off-diagonal element with the same electrodes [73].

For high-speed applications, the traveling-wave Mach-Zehnder modulator (TW-MZM) is commonly used, as shown schematically in Figure 6(a). With a TW-MZM, perfect phase matching between the guided optical wave and the applied electrical (RF) wave is possible, in which case there would be no walkoff between the two waves. In such a device, the modulation bandwidth extends from dc up to some large cutoff frequency, limited only by the impedance mismatch between the load impedance and the characteristic impedance of the TW-MZM, which can be matched by simply changing the load impedance and by the loss of the electrical wave [108], [109]. Recently, two different TW-MZMs using thin-film LN have reached 3-dB electrical modulation bandwidths beyond 100 GHz [18], [72], [110] with $V_{\pi}L$ values of 2.2 V-cm and 6.7 V-cm, respectively. These results compare favorably to conventional LN TW-MZMs, which typically reach a 3-dB electrical modulation bandwidth of about 50 GHz, exceeded only in rare instances, e.g., an EOM defined in bulk LN achieved 70-GHz 3-dB electrical modulation bandwidth at $V_{\pi}L$ of 10.2 V-cm [36].

EOMs in high-speed data communications are designed to operate at wavelengths of 1,310 nm or 1,550 nm, where optical fiber transmission is preferred and laser transceivers are readily available. However, the wide transparency window of LN allows modulators to be designed to operate from the visible up to the mid-infrared (MIR) wavelengths. Visible wavelength modulators are used in free-space communications, NL optics, spectroscopy, and quantum optics [111], while MIR modulators are researched for remote sensing or free space communications [40]. For example, an EOM fabricated on an SiN-LN platform and designed for $\lambda_0 = 674 \text{ nm}$ has a $V_{\pi}L$ of only 0.3 V-cm [111]. Similar MIR modulators will benefit from thin films as well, since bulk-LN modulators are hampered by large mode sizes [40].

Modern high-speed communication channels can support higher-order modulation formats, such as quadratureamplitude modulation (QAM). For a higher-order modulator's device layout, multiple low-bandwidth EOMs can be connected in parallel and driven with multiple voltage levels to reach very high data rates [112]. Due to the size of optical modes in traditional LN waveguides, a high-order QAM transmitter is difficult to realize on a single bulk-LN chip, but could easily fit (including electrical connections) on a 1-cm \times 0.25-cm chip when using thin-film LN technology.

NL OPTICS

NL optical processes can convert optical power between different wavelengths, following the laws of energy conservation

and phase matching. These processes can be used to provide high-power, narrowband light sources at wavelengths at which no adequate laser material exists. They can also be used for other applications, such as filtering, lidar, pulse compression, and single photon sources for quantum optical networks [113]-[117].

A common way to demonstrate the feasibility of a particular material platform for NL optics is second harmonic generation (SHG), which has been demonstrated using LNOI [118]. In the SHG process, two input photons are converted to one output photon at half the wavelength. The efficiency of a second-order NL process, such as SHG, scales quadratically with the optical pump power density, implying that enhanced confinement of light in waveguides will result in more efficient NL optical devices. Traditional waveguides in bulk LN have mode sizes of more than $10 \,\mu\text{m}^2$, while waveguides using LN thin films can support mode sizes smaller than $1 \mu m^2$. As such, a decreased mode size by a factor of ten will result in a 100-fold increase in power conversion efficiency. Some of these efficiency improvements can be sacrificed to significantly reduce the device length to the mm-scale or lower.

The conversion efficiency of an SHG process is characterized by the ratio of output power at the generated wavelength P_{SHG} and the input power at the pump wavelength P_{pump} . As the efficiency scales with the input power and the device

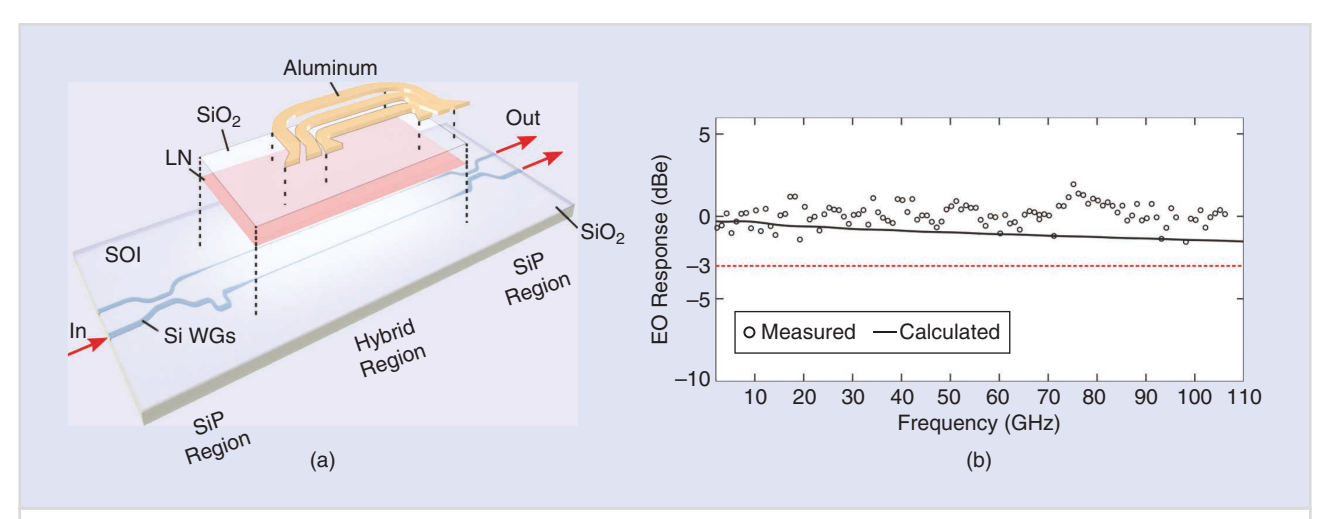


FIGURE 6 (a) A schematic of a hybrid silicon photonics-lithium niobate traveling wave MZI EOM. (b) The electro-optic response extracted from an optical spectrum analyzer measurement is shown. The solid line is the calculated electro-optic response based on the measured RF S-parameters. The measured 1.5-dB electrical modulation bandwidth is reached at 106-GHz modulation frequency and the 3-dB point is estimated beyond 200 GHz [72]. (Source: The Optical Society; reprinted with permission.) SiP: silicon photonics.

length *l* quadratically, it is useful to define a normalized conversion efficiency η as

$$\eta = \frac{P_{\rm SHG}}{P_{\rm pump}^2 l^2}.$$

Record efficiency in bulk up to 150%/(W-cm²) have been demonstrated [119], however many bulk-LN waveguides provide SHG conversion efficiencies typically in the range of 10% to 40%/(W-cm²) [119], [120]. Assume, for example, a 10% lossless conversion of a 1-mW power pump, such as a heterogeneously integrated III-V laser on the silicon photonics platform [121]. A bulk-LN SHG device will require a 31-cm-long bulk-LN waveguide $[\eta = 10\%/(\text{W-cm}^2)]$, which is larger than any bulk-LN wafer, whereas an LN thin-film SHG device could perform this task in about a 3.1-cm-long waveguide $[\eta = 1,000\%/(W-cm^2)]$. This is a realistic length given the available LNOI wafer and die sizes. However, the small bending radii and waveguides offered by LNOI and many hybrid approaches offer novel strategies, beyond just shrinking bulk devices, such as folded structures or resonators. These structures offer not only reduced device length, but also an overall reduced footprint. Figure 7 gives an example for a design of a folded structure. Assuming a 10-time passage through a 1-cm-long NL section and using the design parameters presented in [122], this structure could fit onto just a 10-mm × 0.5-mm footprint including all tapers and bends. In total, this provides a NL section of 10-cm length equal to the standard size of a bulk-LN wafer. The challenges for a structure like this are the precise control of the phases accumulated in the bends and tapers between the NL sections [122], which in turn can potentially benefit from the integration of heaters in a multilayer approach.

Experimental SHG conversion efficiencies as high as 2,600%/(W-cm²) in LN thin-film devices have already been demonstrated [65], promising even smaller devices and higher conversion rates. Given the early state of LN thin-film NL optics technology, further improvement of SHG conversion efficiency and device size is expected by, for example, optimizing mode sizes, reducing propagation losses, or using resonators. Based on these works in second harmonic generation, a number of other NL processes have been demonstrated using LN thin films, further demonstrating the versatility of this platform. These include cascaded second- and third-order frequency conversion [123], cascaded stimulated Raman scattering, second harmonic and difference frequency generation [81], and single photon generation by parametric down conversion [117], [124].

For these frequency conversion processes to be efficient, the correct phase relationship between the interacting beams must be maintained for the complete interaction length, which is usually not fulfilled due to modal or material dispersion. The most common method to do this in both bulk and thin-film LN is by quasi-phase matching (QPM). A nonphase-matched process will still generate converted light. However, the constant buildup of phase mismatch between the beams will lead to a spatially oscillating NL power but no

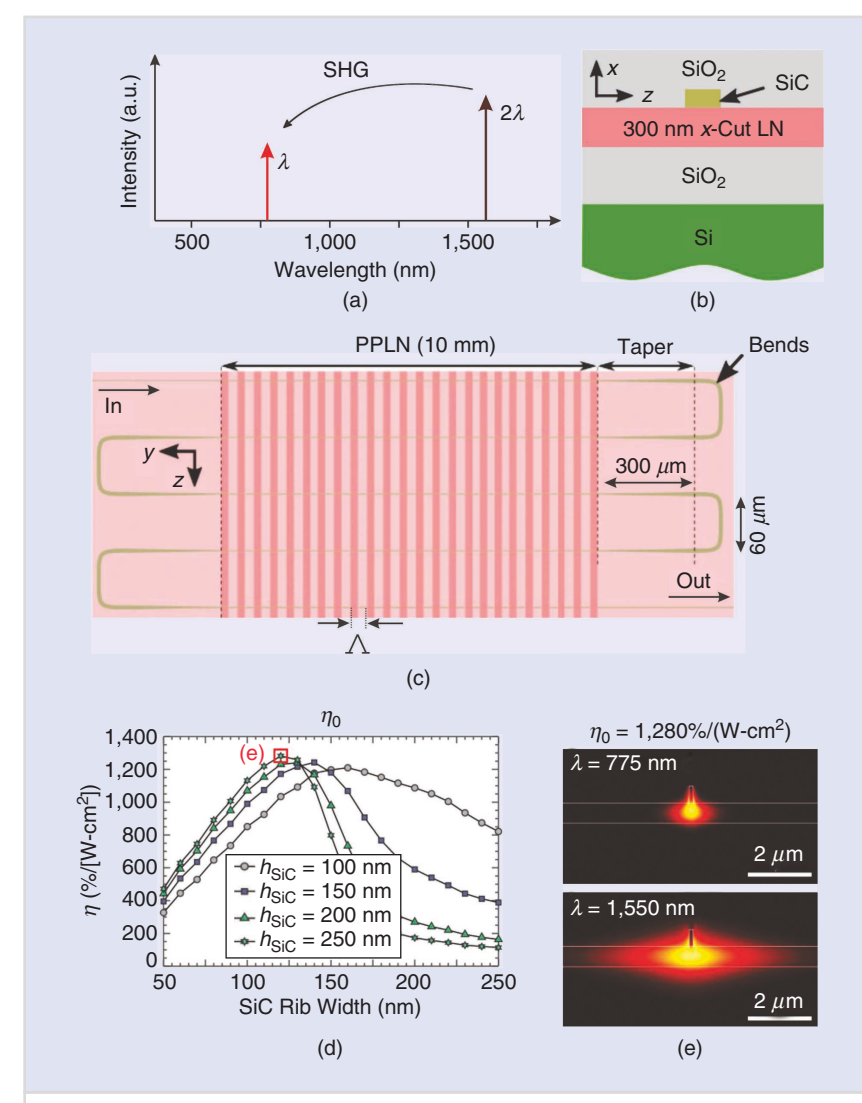


FIGURE 7 (a) A spectral schematic of the second harmonic process showing frequency doubling from 1,550 nm to 775 nm. (b) A cross section of a proposed hybrid silicon carbide (SiC) rib-loaded LNOI frequency doubler. (c) A schematic of the proposed folded structure. Low-loss tapers and bends, which are possible in many LNOI platforms due to the high confinement, enable multiple passes through the nonlinear section. Such a structure can provide the same conversion rates as any traditional bulk-LN device at a much smaller footprint, if the accumulated phases in the bends and tapers are taken into consideration. (d) The simulated conversion efficiencies for different SiC rib heights and widths. (e) The simulated mode profiles of the second harmonic (top) and fundamental (bottom) modes [122]. (Source: The Optical Society; reprinted with permission.) PPLN: periodically poled lithium niobate.

net power buildup. If the phase, however, can be periodically reset within the coherence length, a net power buildup can be achieved. A ferroelectric crystal offers the possible ability to invert the crystal symmetry, and with it the phase of the generated light. Hence, a periodic domain structure can be used to constantly reset the phase mismatch, leading to an efficient conversion process. The exact domain structures, e.g., period length or duty cycle, depends on the desired process and the modal and material dispersion; more complex domain structures, e.g., chirped, can be used to tune the phase-matching process for more complex functionalities, e.g., pulse compression [114].

The mid-infrared wavelength region is particularly promising to further develop thin-film LN NL optics technology. The difference-frequency generation of light is particularly useful in a wavelength regime where direct laser action through uncooled semiconductors is difficult. EOMs that operate at mid-IR wavelengths may achieve uncoupled amplitude and phase modulation performance and at such high speeds are impossible with direct-current modulation of quantum cascade lasers. Conventional electroabsorption semiconductor modulators do not exist at these wavelengths since most materials lack strong (i.e., band-to-band) tunable band modulation in the mid-IR. Furthermore, there are novel device proposals that combine spectroscopy and quantum optics [125] and may realize ultrasensitive spectral measurements of mid-infrared signatures in a highly compact device. Similar to EOM, the LN crystal orientation and light polarization is essential for NL processes. The highest efficiency can be achieved for processes with signal and pump light polarized along the z-axis, which accesses the largest NL tensor element. Therefore, for TE polarized interactions, the x-cut LN is usually chosen. For TM interactions, z-cut LN crystals are usually required [126]. It should be noted that NL interactions can include different polarizations, e.g., the pump beam is TE polarized, while the signal beam is TM polarized. By design, this addresses not the largest tensor element in LN, but such a process is, for example, essential

for birefringence phase-matched schemes, which may not require domain grids.

Domain inversion can, for example, be achieved by electric field poling using electrodes or AFM tips [127], [128]. The structure in Figure 7(c) from [122], for example, would require a poling period of about 2.79 µm for the design with the highest conversion efficiency. To fabricate domain grids, thin films only require moderate poling voltages (>10 V for z-cut; <1,000 V < 1,000 V for x-cut) compared to bulk LN (>10 kV). Here, x- or y-cut films offer the advantage in that they can be poled with (removable) top or side wall electrodes, while z-cut films require buried electrodes that may be difficult to remove and can potentially lead to additional optical loss.

Errors in poling, domain period, or duty cycle can have a great impact on the efficiency and spectral response of a QPM structure and need to be precisely controlled [129]. Further, the additional fabrication step for domain formation may not be desired, or it may be that some structures cannot be poled. It has been reported that ferroelectric domain inversion of z-cut LNOI may be unstable for film thicknesses less than 1 µm [130], but this problem is under investigation [128]. As an alternative to QPM, thin-film waveguides, particularly hybrid structures, can employ mode-dispersion phase matching (MPM), which may be attractive for some applications. In MPM, perfect phase matching between modes of different orders can be achieved [131], leading to an efficient frequency-conversion process for a particular geometry and wavelength. Similarly, ring or WGM resonators can be phase matched without the need for periodic poling [81]. By definition, MPM requires multimode waveguides or resonators, or modes of different polarizations, if a birefringence MPM is targeted.

OTHER DEVICE APPLICATIONS

The rationale for attempting to incorporate LN within a 3D, multilayer device concept, as shown in Figure 1, is that many useful properties of LN are exploited for applications beyond optical communications or data interconnections. In nearly all applications, it seems that using thin-film LN, together with appropriate

focusing and readout structures that are optimized for the highly confined geometry, promises enhanced sensitivity and smaller device footprints compared to bulk-LN based devices. For example, LNOI has been applied as a template for enhanced Raman-based chemical sensing [133], as an electric field sensor [134], and to construct spectrally selective IR sensors operational at room temperature [132], as shown in Figure 8. In this figure, a detector is built from an array of these unit cells. The metamaterial enhances the infrared absorption in a specific spectral range determined by the geometry, leading to a temperature built up in the LNOI. Since LN is pyroelectric, this results in a voltage increase that can be measured between the surface and a back-electrode below the LN.

Given the numerous existing applications of bulk LN, it is likely that we will soon see other applications of LN thin films. For example, the photorefractive effect in LN has long been studied for thermally erasable holographic storage [135], [136], but crosstalk in the bulk geometry has limited practical applications of all-optical memories. These limitations may be overcome in the multilayer thinfilm LN architecture, especially if multiple layers can be stacked.

Similarly, there are applications of LN in optically written gratings for laser resonators [29], and in optical tweezing and surface structuring applications [137]. LN and LN waveguides can be doped with optically active ions, such as erbium or thulium, which can be used to construct optical amplifiers and lasers [29], [30], or single-photon storage memories for quantum repeaters [138], [139]. In recent years, electrically conductive ferroelectric domain walls in LN and many other ferroelectric materials have been discovered. This may lead to a novel type of domain wall electronics and memories [84], [140] that may be mutually beneficial to thin films and multilayer integration [141].

In the RF industry, (bulk) LN has already found its way into consumer products, such as displays and cell phones as a standard material for surface acoustic wave (SAW) and bulk acoustic wave (BAW) RF filters. These filters profit from LN thin films, which promise the

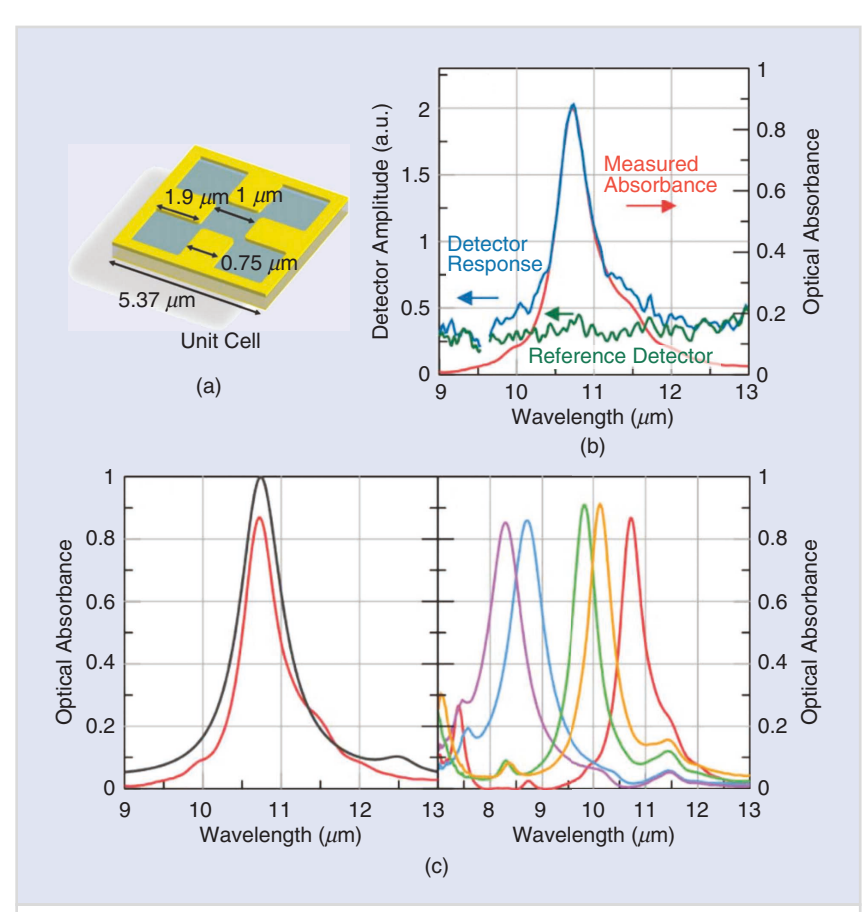


FIGURE 8 (a) A schematic for a single-unit cell of a metamaterial-based IR sensor constructed on LNOI that requires no cooling. (b) The measured absorption curve (red) shows good agreement with the pyroelectric detector response (blue). A measurement with an off-resonant reference detector (green) demonstrates that the metamaterial absorption is essential to the detector's operation. (c) Left: The simulated (black) and experimental (red) wavelength absorption response for a specific detector. Right: The experimental absorption curves for sensors of different geometry showing broad tunability [132]. (Source: The Optical Society; reprinted with permission.)

higher frequencies and smaller device sizes necessary to meet ever-increasing datatransmission demands [44]. Using wafer bonding to achieve a surface acoustic wave LN device integrated with CMOS amplifiers has already been shown [142] and the first SAW filters based on thin-film LN or LT are currently being introduced by RF component manufactures. Thin-film LN also offers new possibilities for the field of acousto-optics, which combines integrated optics and acoustics. Recently, for example, an acoustic gyroscope in thinfilm LN with integrated optical readout was presented [97].

LOOKING FORWARD: CHALLENGES AND OPPORTUNITIES

Optical-quality thin-film LN has been commercially available for less than a decade, unlike its bulk counterpart, and device technology that takes advantage of this new material is making rapid progress. Thin-film LN-based photonic devices recently measured in the laboratory appear to already outclass bulk-LN photonic devices in many applications, including electro-optic modulation and NL frequency conversion. Particularly exciting in the current research context is the combination of technological advancements in silicon photonics over the past two decades with the knowledge gained from nearly 50 years of bulk-LN development, so that the two materials can coexist within the same design and fabrication process flow.

Some roadblocks still exist, both at the individual component level and at the device integration level. Examples of the

former include further reduction of the sidewall roughness of waveguides, especially in resonator structure [64], improved grating couplers and input-ouput efficiency for stand-alone, fiber-coupled devices [80], achieving compact and low-loss waveguide bends for multicomponent integrated optical circuits [28], [72] and improved optical power handling, which benefits nearly every application of LN [65]. Basic research, e.g., improved poling technology and studies of poled domains in thin-film LN devices, must continue alongside technology development [127], [130].

The design of optical components is not just limited to the waveguide cross section but also includes circuit-level issues, whose size and scale stretch the capabilities of conventional simulation software. For example, since conventional LN NL optical devices are quite long and pencil-shaped, in contrast to the typically rectangular form factor of a modern electronics package, improved device layouts for NL optical devices, which are critically enabled by the multilayer approach, are being studied [122].

At the technology frontier, incorporating lasers, detectors, and driver electronics are major challenges for thin-film LN technology to mature into a modern microsystems platform. We have reason for optimism, given the continuing improvement of III-V hybrid laser sources in transceivers [15]. However, the technological roadmap, as in that case, will require substantial and sustained collaboration between fundamental (typically, university) and applied (industrial) researchers. While a similar approach to what is already used in hybrid III-V silicon photonics can perhaps be used to attach laser and detector dies in the same fabrication process as thin-film LN coupon integration, both RF photonics and NL optics typically involve much higher optical powers than digital data communications. In this context, impairment-free optical power transfer between layers and heat dissipation are only two of many challenges that need to be studied carefully. Bonded electronics integration with a thin-film LN optical device, which will be necessary to exploit the extremely high bandwidths of thinfilm LN EOMs already measured, has not been accomplished yet.

Although there are many challenges that must be overcome, in addition to the ones we have listed, the opportunities are even more numerous and exciting. Now, more than at any previous time in the 50-year history of LN as an optical material, the investigation of hybrid and multilayer device design, fabrication, and applications presents an opportunity for foundry-fabricated wafer-scale optical circuits to be integrated into 3D, truly multifunctional integrated circuits. Such microsystems are capable of drastically reducing the size and energy footprint of existing devices, while scaling bandwidths and information-processing capabilities by many orders of magnitude, and supporting new devices that cannot be realized with current technologies.

ACKNOWLEDGMENTS

We acknowledge funding support through Sandia National Laboratories under grant 1856102, the National Science Foundation under grants NSF ECCS-1201308 and EFMA-1640968, and the National Aeronautics and Space Administration under grant NASA NNX16AD14G. Peter O. Weigel acknowledges NDSEG fellowship support.

ABOUT THE AUTHORS

Michael Rüsing (mruesing@eng.ucsd .edu) is with the Department of Electrical and Computer Engineering, University of California, San Diego.

Peter O. Weigel (pweigel@eng.ucsd .edu) is with the Department of Electrical and Computer Engineering, University of California, San Diego.

Jie Zhao (jiz378@eng.ucsd.edu) is with the Department of Electrical and Computer Engineering, University of California, San Diego.

Shayan Mookherjea (smookherjea@ucsd.edu) is with the Department of Electrical and Computer Engineering, University of California, San Diego.

REFERENCES

- J.-Q. Lu, K. Rose, and S. Vitkavage, "3D integration: Why, what, who, when?," Future Fab. Int., vol. 7, no. 23, pp. 25–27, 2007.
- [2] D. T. Spencer et al., "An optical-frequency synthesizer using integrated photonics," *Nature*, vol. 557, no. 7703, pp. 81–85, 2018.
- [3] T. P. Purdy, K. E. Grutter, K. Srinivasan, and J. M. Taylor, "Quantum correlations from a roomtemperature optomechanical cavity," Sci., vol.

- 356, pp. 1265–1268, June 2017. doi: 10.1126/science.aag1407.
- [4] Y. Nitta, J. Ohta, S. Tai, and K. Kyuma, "Optical learning neurochip with internal analog memory," *Appl. Opt.*, vol. 32, no. 8, pp. 1264–1274, 1993. doi: 10.1364/AO.32.001264.
- [5] Y. Shen et al., "Deep learning with coherent nanophotonic circuits," *Nat. Photon.*, vol. 11, pp. 441–446, June 2017. doi:10.1038/nphoton.2017.93.
- [6] A. Politi, M. J. Cryan, J. G. Rarity, S. Yu, and J. L. O'Brien, "Silica-on-silicon waveguide quantum circuits," Sci., vol. 320, no. 5876, pp. 646–649, May 2008. doi: 10.1126/science.1155441.
- [7] A. N. Zorzos, J. Scholvin, E. S. Boyden, and C. G. Fonstad, "Three-dimensional multiwaveguide probe array for light delivery to distributed brain circuits," *Opt. Lett.*, vol. 37, no. 23, pp. 4841–4843, 2012. doi: 10.1364/OL.37.004841.
- [8] M. Lawrence, "Lithium niobate integrated optics," Rep. Prog. Phys., vol. 56, no. 3, pp. 363-429, Mar. 1993. doi: 10.1088/0034-4885/56/3/001.
- [9] J. Lv, Y. Cheng, W. Yuan, X. Hao, and F. Chen, "Three-dimensional femtosecond laser fabrication of waveguide beam splitters in LiNbO₃ crystal," Opt. Mater. Express, vol. 5, no. 6, pp. 1274–1280, 2015. doi: 10.1364/OME.5.001274.
- [10] M. Li, W. H. P. Pernice, C. Xiong, T. Baehr-Jones, M. Hochberg, and H. X. Tang, "Harnessing optical forces in integrated photonic circuits," *Nature*, vol. 456, pp. 480–484, Nov. 2008. doi: 10.1038/nature07545.
- [11] J. Sun, E. Timurdogan, A. Yaacobi, E. S. Hosseini, and M. R. Watts, "Large-scale nanophotonic phased array," *Nature*, vol. 493, pp. 195–199, Jan. 2013. doi: 10.1038/nature11727.
- [12] C. Sun et al., "Single-chip microprocessor that communicates directly using light," *Nature*, vol. 528, pp. 534–538, Dec. 2015. doi: 10.1038/ nature16454.
- [13] C. Zhang, S. Zhang, J. D. Peters, and J. E. Bowers, "8 × 8 × 40 Gbps fully integrated silicon photonic network on chip," *Optica*, vol. 3, no. 7, pp. 785–786, July 2016. doi: 10.1364/OPTI-CA.3.000785.
- [14] E. Bernier et al., "Large-scale silicon photonic switch," in *Proc. Optical Fiber Communication Conf.*, Washington, DC, USA, 2018, p. Th1J.1.
- [15] Z. Wang et al., "Novel light source integration approaches for silicon photonics," *Laser Photon. Rev.*, vol. 11, no. 4, p. 1700063, July 2017. doi: 10.1002/lpor.201700063.
- [16] K.-H. Luo et al., "Direct generation of genuine single-longitudinal-mode narrowband photon pairs," New J. Phys., vol. 17, no. 7, p. 073039, Aug. 2015. doi: 10.1088/1367-2630/17/7/073039.
- [17] M. Bazzan and C. Sada, "Optical waveguides in lithium niobate: Recent developments and applications," Appl. Phys. Rev. vol. 2, no. 4, p. 40603, Dec. 2015. doi: 10.1063/1.4931601.
- [18] C. Wang et al., "Integrated lithium niobate electro-optic modulators operating at CMOS-compatible voltages," *Nature*, vol. 562, pp. 101–104, Sept. 2018. doi: 10.1038/s41586-018-0551-y.
- [19] M. F. Volk, S. Suntsov, C. E. Rüter, and D. Kip, "Low loss ridge waveguides in lithium niobate thin films by optical grade diamond blade dicing," Opt. Express, vol. 24, no. 2, pp. 1386–1391, Jan. 2016. doi: 10.1364/OE.24.001386.
- [20] Y. A. Vlasov and S. McNab, "Losses in single-mode silicon-on-insulator strip waveguides and bends," *Opt. Express*, vol. 12, no. 8, pp. 1622–1631, 2004. doi: 19474988.
- [21] J. R. Ong, R. Kumar, R. Aguinaldo, and S. Mookherjea, "Efficient CW four-wave mixing in silicon-on-insulator micro-rings with active carrier removal," *IEEE Photon. Technol. Lett.*, vol. 25, no. 17, pp. 1699–1702, Sept. 2013. doi: 10.1109/LPT.2013.2272521.
- [22] L. Ottaviano, M. Pu, E. Semenova, and K. Yvind, "Low-loss high-confinement waveguides and

- microring resonators in AlGaAs-on- insulator," *Opt. Lett.*, vol. 41, no. 17, pp. 3996–3999, Sept. 2016. doi: 10.1364/OL.41.003996.
- [23] P. Rabiei, J. Ma, S. Khan, J. Chiles, and S. Fath-pour, "Heterogeneous lithium niobate photonics on silicon substrates," *Opt. Express*, vol. 21, no. 21, pp. 25573–25581, 2013. doi: 10.1364/OE.21.025573.
- [24] K. Dolgaleva, W. C. Ng, L. Qian, and J. S. Aitchison, "Compact highly-nonlinear AlGaAs waveguides for efficient wavelength conversion," Opt. Express, vol. 19, no. 13, pp. 12440–12455, 2011. doi: 10.1364/OE.19.012440.
- [25] S. Saeidi, K. M. Awan, L. Sirbu, and K. Dolgaleva, "Nonlinear photonics-on-a-chip in III-V semiconductors: Quest for promising material candidates," *Appl. Opt.*, vol. 56, no. 19, pp. 5532–5541, July 2017. doi: 10.1364/AO.56.005532.
- [26] L. Cai, R. Kong, Y. Wang, and H. Hu, "Channel waveguides and y-junctions in x-cut single-crystal lithium niobate thin film," *Opt. Express*, vol. 23, no. 22, pp. 29211–29221, Nov. 2015. doi: 10.1364/OE.23.029211.
- [27] P. O. Weigel et al., "Lightwave circuits in lithium niobate through hybrid waveguides with silicon photonics," Sci. Rep., vol. 6, pp. 1–9, Mar. 2016.
- [28] X. P. Li, K. X. Chen, and Z. F. Hu, "Low-loss bent channel waveguides in lithium niobate thin film by proton exchange and dry etching," *Opt. Mater. Express*, vol. 8, no. 5, pp. 1322–1327, May 2018. doi: 10.1364/OME.8.001322.
- [29] W. Sohler et al., "Erbium-doped lithium niobate waveguide lasers," *IEICE Trans. Electron.*, vol. E88-C, no. 5, pp. 990–997, May 2005. doi: 10.1093/ietele/e88-c.5.990.
- [30] C. E. Rüter et al., "Characterization of diced ridge waveguides in pure and Er-doped lithium-niobate-on-insulator (LNOI) substrates," Proc. SPIE, vol. 8982, Mar. 2014. doi: 10.1117/12.2036270.
- [31] O. Marshall et al., "Heterogeneous integration on silicon photonics," *Proc. IEEE*, vol. 106, no. 12, pp. 2258–2269, Dec. 2018. doi: 10.1109/JPROC.2018.2858542.
- [32] G. Roelkens et al., "III-V/silicon photonics for on-chip and intra-chip optical interconnects," *Laser Photonics Rev.*, vol. 4, no. 6, pp. 751–779, Nov. 2010. doi: 10.1002/lpor.200900033.
- [33] L. Cao, A. Aboketaf, Z. Wang, and S. Preble, "Hybrid amorphous silicon (a-Si:H)–LiNbO3 electro-optic modulator," Opt. Commun., vol. 330, pp. 40–44, Nov. 2014. doi: 10.1016/j.opt-com.2014.05.021.
- [34] C. Xiong et al., "Aluminum nitride as a new material for chip-scale optomechanics and nonlinear optics," New J. Phys., vol. 14, no. 9, p. 095014, Sept. 2012. doi: 10.1088/1367-2630/14/9/095014.
- [35] A. Majkic et al., "Optical nonlinear and electrooptical coefficients in bulk aluminium nitride single crystals," *Physica Status Solidi (B) Basic Res.*, vol. 254, no. 9, 2017. doi: 10.1002/pssb.201700077.
- [36] K. Noguchi, O. Mitomi, and H. Miyazawa, "Millimeter-wave Ti:LiNbO₃ optical modulators," *J. Lightwave Technol.*, vol. 16, no. 4, pp. 615–619, Apr. 1998. doi: 10.1109/50.664072.
- [37] S. Lange et al., "100 GBd intensity modulation and direct detection with an InP-based monolithic DFB laser Mach-Zehnder modulator," J. Lightwave Technol., vol. 36, no. 1, pp. 97–102, 2017. doi: 10.1109/JLT.2017.2743211.
- [38] G. T. Reed, G. Mashanovich, F. Y. Gardes, and D. J. Thomson, "Silicon optical modulators," Nat. Photonics, vol. 4, pp. 518–526, Aug. 2010. doi: 10.1038/nphoton.2010.179.
- [39] L. Chang et al., "Heterogeneously integrated GaAs waveguides on insulator for efficient frequency conversion," *Laser Photonics Rev.*, vol. 12, no. 10, pp. 1-7, 2018. doi: 10.1002/ lpor.201800149.
- [40] J. Chiles and S. Fathpour, "Mid-infrared integrated waveguide modulators based on silicon-on-lithium-niobate photonics," *Optica*, vol. 1, no. 5,

- pp. 350–355, Nov. 2014. doi: 10.1364/OPTI-CA.1.000350.
- [41] R. S. Weis and T. K. Gaylord, "Lithium niobate: Summary of physical properties and crystal structure," *Appl. Phys. A*, vol. 37, no. 4, pp. 191–203, Aug. 1985. doi: 10.1007/BF00614817.
- [42] W. Sohler et al., "Integrated optical devices in lithium niobate," Opt. Photonics News, vol. 19, no. 1, pp. 24–31, Jan. 2008. doi: 10.1364/ OPN.19.1.000024.
- [43] S. Miyazawa, "Growth of LiNbO₃ single-crystal film for optical waveguides," *Appl. Phys. Lett.*, vol. 23, no. 4, pp. 198–200, Aug. 1973. doi: 10.1063/1.1654857.
- [44] A. Bartasyte, S. Margueron, T. Baron, S. Oliveri, and P. Boulet, "Toward high-quality epitaxial LiNbO₃ and LiTaO₃ thin films for acoustic and optical applications," *Adv. Mater. Interfaces*, vol. 4, no. 8, p. 1600998, Apr. 2017. doi: 10.1002/admi.201600998.
- [45] M. Levy et al. "Fabrication of single-crystal lithium niobate films by crystal ion slicing," *Appl. Phys. Lett.*, vol. 73, pp. 2293–2295, Oct. 1998. doi: 10.1063/1.121801.
- [46] G. Poberaj, H. Hu, W. Sohler, and P. Günter, "Lithium niobate on insulator (LNOI) for microphotonic devices," *Laser Photonics Rev.*, vol. 6, no. 4, pp. 488–503, Jul. 2012. doi: 10.1002/ lpor.201100035.
- [47] V. Stenger, M. Shnider, S. Sriram, D. Dooley, and M. Stout, "Thin film lithium tantalate (TFLT) pyroelectric detectors," *Proc. SPIE*, vol. 82610, p. 82610Q, Feb. 2012. doi: 10.1117/12.908523.
- [48] M. Rüsing et al., "Vibrational properties of LiN b_{1-x}Ta_xO₃ mixed crystals," *Phys. Rev. B*, vol. 93, no. 18, p. 184305, 2016.
- [49] R. V. Schmidt and I. P. Kaminow, "Metal-diffused optical waveguides in LiN bO₃," Appl. Phys. Lett., vol. 25, pp. 458–460, Oct. 1974. doi: 10.1063/1.1655547.
- [50] J. L. Jackel, C. E. Rice, and J. J. Veselka, "Proton exchange for high-index waveguides in LiNbO₃," *Appl. Phys. Lett.*, vol. 41, no. 7, pp. 607–608, 1982. doi: 10.1063/1.93615.
- [51] P. G. Suchoski, T. K. Findakly, and F. J. Leonberger, "Stable low-loss proton-exchanged LiNbO3 waveguide devices with no electro-optic degradation," *Opt. Lett.*, vol. 13, no. 11, pp. 1050–1052, 1988. doi: 10.1364/OL.13.001050.
- [52] Y. N. Korkishko et al., "Reverse proton exchange for buried waveguides in LiNbO₃," *J. Opt. Soc. Am. A*, vol. 15, no. 7, pp. 1838–1842, 1998. doi: 10.1364/JOSAA.15.001838.
- [53] L. Cai, Y. Wang, and H. Hu, "Low-loss wave-guides in a single-crystal lithium niobate thin film," *Opt. Lett.*, vol. 40, no. 13, pp. 3013–3016, July 2015. doi: 10.1364/OL.40.003013.
- [54] A. Boes, B. Corcoran, L. Chang, J. Bowers, and A. Mitchell, "Status and potential of lithium niobate on insulator (LNOI) for photonic integrated circuits," *Laser Photon. Rev.*, vol. 12, no. 4, p. 1700256, Feb. 2018. doi: 10.1002/ lpor.201700256.
- [55] S.-M. Zhang, Y.-P. Jiang, and Y. Jiao, "Clean waveguides in lithium niobate thin film formed by He ion implantation," *Appl. Phys. B*, vol. 123, no. 8, p. 220, Aug. 2017.
- [56] J. Thomas et al., "Laser direct writing: Enabling monolithic and hybrid integrated solutions on the lithium niobate platform," *Physica Status Solidi* (A), vol. 208, no. 2, pp. 276–283, Feb. 2011. doi: 10.1002/pssa.201026452.
- [57] H. Jin et al., "On-chip generation and manipulation of entangled photons based on reconfigurable lithium-niobate waveguide circuits," *Phys. Rev. Lett.*, vol. 113, p. 103601, Sept. 2014. doi: 10.1103/PhysRevLett.113.103601.
- [58] A. J. Mercante et al., "Thin film lithium niobate electro-optic modulator with terahertz operating bandwidth," *Opt. Express*, vol. 26, no. 11, pp. 14810–14816, May 2018. doi: 10.1364/ OE.26.014810.

- [59] G. Ulliac et al., "Ultra-smooth LiNbO3 micro and nano structures for photonic applications," *Microelectron. Eng.*, vol. 88, no. 8, pp. 2417–2419, Aug. 2011. doi: 10.1016/j. mec.2011.02.024.
- [60] M. Zhang, C. Wang, R. Cheng, A. Shams-Ansari, and M. Lončar, "Monolithic ultra-high-Q lithium niobate microring resonator," *Optica*, vol. 4, no. 12, p. 1536, Dec. 2017.
- [61] C. Wang, M. Zhang, B. Stern, M. Lipson, and M. Lončar, "Nanophotonic lithium niobate electro-optic modulators," *Opt. Express*, vol. 26, no. 2, pp. 1547–1555, Jan. 2018. doi: 10.1364/ OE.26.001547.
- [62] I. Krasnokutska, J.-L. J. Tambasco, X. Li, and A. Peruzzo, "Ultra-low loss photonic circuits in lithium niobate on insulator," *Opt. Express*, vol. 26, no. 2, pp. 897–904, Jan. 2018. doi: 10.1364/ OE.26.000897.
- [63] H. Hu, R. Ricken, and W. Sohler, "Lithium niobate photonic wires," *Opt. Express*, vol. 17, no. 26, pp. 24261–24268, Dec. 2009. doi: 10.1364/ OE.17.024261.
- [64] R. Wolf, I. Breunig, H. Zappe, and K. Buse, "Scattering-loss reduction of ridge waveguides by sidewall polishing," *Opt. Express*, vol. 26, no. 16, pp. 19815–19820, Aug. 2018. doi: 10.1364/ OE.26.019815.
- [65] C. Wang et al., "Ultrahigh-efficiency wavelength conversion in nanophotonic periodically poled lithium niobate waveguides," *Optica*, vol. 5, no. 11, p. 1438, 2018. doi: 10.1364/OPTICA.5.001438.
- [66] S. Li, L. Cai, Y. Wang, Y. Jiang, and H. Hu, "Waveguides consisting of single-crystal lithium niobate thin film and oxidized titanium stripe," *Opt. Express*, vol. 23, no. 19, pp. 24212–24219, Sept. 2015. doi: 10.1364/OE.23.024212.
- [67] L. Chang et al., "Heterogeneous integration of lithium niobate and silicon nitride waveguides for wafer-scale photonic integrated circuits on silicon," Opt. Lett., vol. 42, no. 4, pp. 803–806, Feb. 2017. doi: 10.1364/OL.42.000803.
- [68] A. Rao et al., "Heterogeneous microring and Mach-Zehnder modulators based on lithium niobate and chalcogenide glasses on silicon," Opt. Express, vol. 23, no. 17, pp. 22746–22752, Aug. 2015. doi: 10.1364/OE.23.022746.
- [69] Y. Wang et al., "Amorphous silicon-lithium niobate thin film strip-loaded waveguides," Opt. Mater. Express, vol. 7, no. 11, pp. 4018–4028, Oct. 2017. doi: 10.1364/OME.7.004018.
- [70] M. Hayrinen et al., "Low-loss titanium dioxide strip waveguides fabricated by atomic layer deposition," J. Lightw. Technol., vol. 32, no. 2, pp. 208– 212, Jan. 2014. doi: 10.1109/JLT.2013.2291960.
- [71] M. M. R. Howlader, T. Suga, and M. J. Kim, "Room temperature bonding of silicon and lithium niobate," *Appl. Phys. Lett.*, vol. 89, pp. 31914, July 2006.
- [72] P. O. Weigel et al., "Bonded thin film lithium niobate modulator on a silicon photonics platform exceeding 100 GHz 3-dB electrical modulation bandwidth," Opt. Express, vol. 26, no. 18, pp. 23728–23739, Sept. 2018. doi: 10.1364/ OE.26.023728.
- [73] L. Chen, Q. Xu, M. G. Wood, and R. M. Reano, "Hybrid silicon and lithium niobate electrooptical ring modulator," *Optica*, vol. 1, no. 2, pp. 112–118, Aug. 2014. doi: 10.1364/OPTI-CA.1.000112.
- [74] D. Tulli, D. Janner, and V. Pruneri, "Room temperature direct bonding of LiNbO3 crystal layers and its application to high-voltage optical sensing," J. Micromech. Microeng., vol. 21, no. 8, p. 85025, 2011.
- [75] J. D. Witmer, J. A. Valery, P. Arrangoiz-Arriola, C. J. Sarabalis, J. T. Hill, and A. H. Safavi-Naeini, "High-Q photonic resonators and electro-optic coupling using silicon-on-lithium-niobate," *Scien-tific Rep.*, vol. 7, Art. no. 46313, Dec. 2017. doi: 10.1038/srep46313.
- [76] P. O. Weigel and S. Mookherjea, "Reducing the thermal stress in a heterogeneous material stack

- for large-area hybrid optical silicon-lithium niobate waveguide micro-chips," *Opt. Mater.*, vol. 66, pp. 605–610, Apr. 2017. doi: 10.1016/j.opt-mat.2017.03.014.
- [77] W. D. Sacher et al., "Tri-layer silicon nitride-onsilicon photonic platform for ultra-low-loss crossings and interlayer transitions," *Opt. Express*, vol. 25, no. 25, pp. 30862–30875, Dec. 2017. doi: 10.1364/OE.25.030862.
- [78] W. D. Sacher et al., "Monolithically integrated multilayer silicon nitride-on-silicon waveguide platforms for 3-D photonic circuits and devices," *Proc. IEEE*, vol. 106, no. 12, pp. 2232–2245. Dec. 2018. doi: 10.1109/JPROC.2018.2860994.
- [79] J. Wang et al., "High-Q lithium niobate microdisk resonators on a chip for efficient electrooptic modulation," Opt. Express, vol. 23, no. 18, pp. 23072–23078, Sept. 2015. doi: 10.1364/ OE.23.023072.
- [80] Z. Chen, R. Peng, Y. Wang, H. Zhu, and H, Hu, "Grating coupler on lithium niobate thin film waveguide with a metal bottom reflector," Opt. Mater. Express, vol. 7, no. 11, pp. 4010–4017, Nov. 2017. doi: 10.1364/OME.7.004010.
- [81] R. Wolf, I. Breunig, H. Zappe, and K. Buse, "Cascaded second-order optical nonlinearities in on-chip micro rings," *Opt. Express*, vol. 25, no. 24, pp. 29927–29933, Nov. 2017. doi: 10.1364/ OE.25.029927.
- [82] H. Liang, R. Luo, Y. He, H. Jiang, and Q. Lin, "High-quality lithium niobate photonic crystal nanocavities," *Optica*, vol. 4, no. 10, pp. 1251–1258, Oct. 2017. doi: 10.1364/OPTI-CA.4.001251.
- [83] X. P. Li, K. X. Chen, and L. F. Wang, "Compact and electro-optic tunable interleaver in lithium niobate thin film," Opt. Lett., vol. 43, no. 15, pp. 3610–3613, July 2018. doi: 10.1364/OL.43.003610.
- [84] P. S. Bednyakov, B. I. Sturman, T. Sluka, A. K. Tagantsev, and P. V. Yudin, "Physics and applications of charged domain walls," npj Comput. Mater., vol. 4, no. 4, p. 65, Nov. 2018.
- [85] A. Guarino, G. Poberaj, D. Rezzonico, R. Degl'Innocenti, and P. Günter, "Electro-optically tunable microring resonators in lithium niobate," *Nat. Photon.*, vol. 1, pp. 407–410, July 2007. doi: 10.1038/nphoton.2007.93.
- [86] T.-J. Wang, C.-H. Chu, and C.-Y. Lin, "Electrooptically tunable microring resonators on lithium niobate," Opt. Lett., vol. 32, no. 19, pp. 2777– 2779, Oct. 2007. doi: 10.1364/OL.32.002777.
- [87] L. Chen, M. G. Wood, and R. M. Reano, "12.5 pm/V hybrid silicon and lithium niobate optical microring resonator with integrated electrodes," *Opt. Express*, vol. 21, no. 22, pp. 27003– 27010, Oct. 2013. doi: 10.1364/OE.21.027003.
- [88] Y. S. Lee, G.-D. Kim, W.-J. Kim, S.-S. Lee, W.-G. Lee, and W. H. Steier, "Hybrid Si-LiNbO₃ microring electro-optically tunable resonators for active photonic devices," *Opt. Lett.*, vol. 36, no. 7, pp. 1119–1121, Apr. 2011. doi: 10.1364/ OL.36.001119.
- [89] L. Chen, J. Chen, J. Nagy, and R. M. Reano, "Highly linear ring modulator from hybrid silicon and lithium niobate," *Opt. Express*, vol. 23, no. 10, pp. 13255–13264, May 2015. doi: 10.1364/ OE.23.013255.
- [90] M. Zhang, C. Wang, B. Buscaino, A. Shams-Ansari, J. M. Kahn, and M. Loncar, "Electro-optic frequency comb generation in ultrahigh-Q integrated lithium niobate micro-resonators," in Proc. OSA Conf. Lasers and Electro-Optics, Washington, DC, p. FW3E.4, 2018. [Online]. Available: https://doi.org/10.1364/CLEO_QELS.2018.FW3E.4.
- [91] X. Zhu et al., "4 × 44 Gb/s packet-level switching in a second-order microring switch," *IEEE Photon. Technol. Lett.*, vol. 24, no. 17, pp. 1555–1557, Sept. 2012. doi: 10.1109/LPT.2012.2208947.
- [92] H. Jiang, H. Liang, R. Luo, X. Chen, Y. Chen, and Q. Lin, "Nonlinear frequency conversion in one dimensional lithium niobate photonic crystal

- nanocavities," *Appl. Phys. Lett.*, vol. 113, no. 2, p. 021104, July 2018. doi: 10.1063/1.5039948.
- [93] S. M. Zhang, L. T. Cai, Y. P. Jiang, and Y. Jiao, "High extinction ratio bandgap of photonic crystals in LNOI wafer," *Opt. Mater.*, vol. 64, pp. 203–207, Feb. 2017. doi: 10.1016/j.optmat.2016.12.017.
- [94] E. Saitoh, Y. Kawaguchi, K. Saitoh, and M. Koshiba, "TE/TM-pass polarizer based on lithium niobate on insulator ridge waveguide," *IEEE Photon. J.*, vol. 5, no. 2, seq. no. 6600610, Apr. 2013. doi: 10.1109/JPHOT.2013.2250938.
- [95] Z. Gong et al., "Optimal design of dc-based polarization beam splitter in lithium niobate on insulator," *Opt. Commun.*, vol. 396, pp. 23–27, Aug. 2017. doi: 10.1016/j.optcom.2017.03.028.
- [96] Z. Chen, Y. Wang, Y. Jiang, R. Kong, and H. Hu, "Grating coupler on single-crystal lithium niobate thin film," *Opt. Mater.*, vol. 72, pp. 136–139, Oct. 2017. doi: 10.1016/j.optmat.2017.05.061.
- [97] M. Mahmoud et al., "Novel on chip rotation detection based on the acousto-optic effect in surface acoustic wave gyroscopes," *Opt. Express*, vol. 26, pp. 25060, Sept. 2018. doi: 10.1364/ OE.26.025060.
- [98] K. Suzuki, T. Yamada, O. Moriwaki, H. Takahashi, and M. Okuno, "Polarization-insensitive operation of lithium niobate Mach-Zehnder interferometer with silica PLC-based polarization diversity circuit," *IEEE Photon. Technol. Lett.*, vol. 20, no. 10, pp. 773–775, May 2008. doi: 10.1109/LPT.2008.921109.
- [99] K. Shang, S. Pathak, B. Guan, G. Liu, and S. J. B. Yoo, "Low-loss compact multilayer silicon nitride platform for 3D photonic integrated circuits," *Opt. Express*, vol. 23, no. 16, pp. 21334–21342, Aug. 2015. doi: 10.1364/OE.23.021334.
- [100] R. Takei, Y. Maegami, E. Omoda, Y. Sakakibara, M. Mori, and T. Kamei, "Low-loss and low wavelength-dependence vertical inter-layer transition for 3D silicon photonics," *Opt. Express*, vol. 23, no. 14, pp. 18602–18610, July 2015. doi: 10.1364/OE.23.018602.
- [101] M. Sodagar, R. Pourabolghasem, A. A. Eftekhar, and A. Adibi, "High-efficiency and wideband interlayer grating couplers in multilayer Si/ SiO₂/SiN platform for 3D integration of optical functionalities," *Opt. Express*, vol. 22, no. 14, pp. 16767–16777, July 2014. doi: 10.1364/ OE.22.016767.
- [102] X. Zheng et al., "Optical proximity communication using reflective mirrors," Opt. Express, vol. 16, no. 19, pp. 15052–15058, Sept. 2008. doi: 10.1364/OE.16.015052.
- [103] A. N. R. Ahmed, A. Mercante, S. Shi, P. Yao, and D. W. Prather, "Vertical mode transition in hybrid lithium niobate and silicon nitride-based photonic integrated circuit structures," *Opt. Lett.*, vol. 43, no. 17, pp. 4140–4143, Sept. 2018. doi: 10.1364/ OL.43.004140.
- [104] P. O. Weigel et al., Hybrid silicon photoniclithium niobate electro-optic Mach-Zehnder modulator beyond 100 GHz bandwidth, arXiv:1803.10365, pp. 1–19, Mar. 2018.
- [105] H. Hui, R. Ricken, and W. Sohler, "Etching of lithium niobate: From ridge waveguides to photonic crystal structures," in *Proc. ECOC* 2008, p. WeD3. [Online]. Available: https:// www.ecio-conference.org/wp-content/ uploads/2016/05/2008/2008_WeD3.pdf
- [106] E. Wooten et al., "A review of lithium niobate modulators for fiber-optic communications systems," *IEEE J. Sel. Topics Quantum Electron.*, vol. 6, no. 1, pp. 69–82, Jan./Feb. 2000. doi: 10.1109/2944.826874.
- [107] A. Rao and S. Fathpour, "Compact lithium niobate electrooptic modulators," *IEEE J. Sel. Topics Quantum Electron.*, vol. 24, no. 4, seq. no. 3400114, July 2018. doi: 10.1109/ISTOE.2017.2779869.
- [108] G. Ghione, Semiconductor Devices for High-Speed Optoelectronics. Cambridge, U.K.: Cambridge Univ. Press, 2009.

- [109] W. S. C. Chang, Ed., RF Photonic Technology in Optical Fiber Links. Cambridge, U.K.: Cambridge Univ. Press, 2002.
- [110] M. Zhang et al., "Ultra-high bandwidth integrated lithium niobate modulators with record-low Vπ," in *Proc. OSA Optical Fiber Communication Conf.*, Washington, DC, 2018, p. Th4A.5.
- [111] K. K. Mehta, G. N. West, and R. J. Ram, "SiN-on-LiNbO₃ integrated optical modulation at visible," in *Proc. OSA Conf. Lasers and Electro-Optics*, Washington, DC, 2017, p. STu3N.7.
- [112] T. Kawanishi, "Parallel Mach–Zehnder modulators for quadrature amplitude modulation," *IEICE Electron. Express*, vol. 8, no. 20, pp. 1678– 1688, 2011. doi: 10.1587/elex.8.1678.
- [113] M. Allgaier et al., "Highly efficient frequency conversion with bandwidth compression of quantum light," *Nature Commun.*, vol. 8, Art. no. 14288, 2017. doi: 10.1038/ncomms14288.
- [114] G. Imeshev et al., "Ultrashort-pulse secondharmonic generation with longitudinally nonuniform quasi-phase-matching gratings: Pulse compression and shaping: Errata," J. Opt. Soc. Am. B, vol. 18, no. 1, p. 121, Jan. 2001. doi: 10.1364/ JOSAB.18.000121.
- [115] E. Garmire, "Nonlinear optics in daily life," Opt. Express, vol. 21, no. 25, pp. 30532–30544, Dec. 2013. doi: 10.1364/OE.21.030532.
- [116] P. R. Sharapova et al., "Toolbox for the design of LiNbO₃-based passive and active integrated quantum circuits," *New J. Phys.*, vol. 19, no. 12, p. 123009, Dec. 2017. doi: 10.1088/1367-2630/ aa9033.
- [117] A. Rao et al., "Photon pair generation on a silicon chip using nanophotonic periodicallypoled lithium niobate waveguides," in Proc. CLEO 2018, 2018, pp. 1–2. [Online]. Available: https://ieeexplore.ieee.org/document/ 8427046
- [118] R. Geiss et al., "Fabrication of nanoscale lithium niobate waveguides for second-harmonic generation," Opt. Lett., vol. 40, no. 12, pp. 2715–2718, 2015. doi: 10.1364/OL.40.002715.
- [119] K. R. Parameswaran, R. K. Route, J. R. Kurz, R. V. Roussev, M. M. Fejer, and M. Fujimura, "Highly efficient second-harmonic generation in buried waveguides formed by annealed and reverse proton exchange in periodically poled lithium niobate," *Opt. Lett.*, vol. 27, no. 3, pp. 179– 181, Feb. 2002. doi: 10.1364/OL.27.000179.
- [120] L. Gui, H. Hu, M. Garcia-Granda, and W. Sohler, "Local periodic poling of ridges and ridge waveguides on X- and Y-Cut LiNbO3 and its application for second harmonic generation," Opt. Express, vol. 17, no. 5, pp. 3923–3928, Mar. 2009. doi: 10.1364/OE.17.003923.
- [121] X. Wang et al., "Photon pair generation using a silicon photonic hybrid laser," APL Photon., vol. 3, no. 10, pp. 106104, 2018. doi: 10.1063/1.5040118.
- [122] P. O. Weigel and S. Mookherjea, "Design of folded hybrid silicon carbide-lithium niobate waveguides for efficient second-harmonic generation," *J. Opt. Soc. Am. B*, vol. 35, pp. 593, Mar. 2018. doi: 10.1364/JOSAB.35.000593.
- [123] A. Honardoost et al., "Cascaded integration of optical waveguides with third-order nonlinearity with lithium niobate waveguides on silicon substrates," *IEEE Photon. J.*, vol. 10, pp. 1–9, June 2018. doi: 10.1109/JPHOT.2018.2827995.
- [124] R. Luo, H. Jiang, S. Rogers, H. Liang, Y. He, and Q. Lin, "On-chip second-harmonic generation and broadband parametric down-conversion in a lithium niobate microresonator," *Opt. Express*, vol. 25, pp. 24531, Sept. 2017. doi: 10.1364/ OE.25.024531.
- [125] A. S. Solntsev, P. Kumar, T. Pertsch, A. A. Sukhorukov, and F. Setzpfandt, "LiNbO₃ waveguides for integrated SPDC spectroscopy," APL Photon., vol. 3, no. 2, pp. 021301, 2018. doi: 10.1063/1.5009766.
- [126] M. Chauvet et al., "Periodically poled LiNbO₃ ridge waveguides on silicon for second-harmonic

- generation," *Proc. SPIE*, vol. 9891, p. 98910S, May 2016. doi: 10.1117/12.2228083.
- [127] P. Mackwitz, M. Rüsing, G. Berth, A. Widhalm, K. Müller, and A. Zrenner, "Periodic domain inversion in x-cut single-crystal lithium niobate thin film," *Appl. Phys. Lett.*, vol. 108, no. 15, p. 152902, Apr. 2016. doi: 10.1063/1.4946010.
- [128] T. R. Volk, R. V. Gainutdinov, and H. H. Zhang, "Domain-wall conduction in AFM-written domain patterns in ion-sliced LiNbO₃ films," Appl. Phys. Lett., vol. 110, no. 13, p. 132905, Mar. 2017. doi: 10.1063/1.4978857.
- [129] M. Fejer, G. Magel, D. Jundt, and R. Byer, "Quasi-phase-matched second harmonic generation: Tuning and tolerances," *IEEE J. Quantum Electron.*, vol. 28, no. 11, pp. 2631–2654, Nov. 1992. doi: 10.1109/3.161322.
- [130] G.-H. Shao et al., "Ferroelectric domain inversion and its stability in lithium niobate thin film on insulator with different thicknesses," AIP Adv., vol. 6, no. 7, p. 075011, July 2016. Doi: 10.1063/1.4959197.
- [131] L. Cai, A. V. Gorbach, Y. Wang, H. Hu, and W. Ding, "Highly efficient broadband second harmonic generation mediated by mode hybridization and nonlinearity patterning in compact fiber-integrated lithium niobate nano-waveguides," Sci. Rep., vol. 8, no. 1, Art. no. 12478, 2018. [Online]. Available: https://www.nature.com/articles/s41598-018-31017-0
- [132] J. Y. Suen et al., "Multifunctional metamaterial pyroelectric infrared detectors," *Optica*, vol. 4, no. 2, pp. 276–279, Feb. 2017. doi: 10.1364/ OPTICA.4.000276.
- [133] R. M. Al-Shammari et al., "Photoinduced enhanced Raman from lithium niobate on insulator template," ACS Appl. Mater. Interfaces, vol. 10, no. 36, pp. 30871–30878, Aug. 2018. doi: 10.1021/acsami.8b10076.
- [134] L. Chen and R. M. Reano, "Compact electric field sensors based on indirect bonding of lithium niobate to silicon microrings," *Opt. Express*, vol. 20, no. 4, pp. 4032–4038, Feb. 2012. doi: 10.1364/OE.20.004032.
- [135] K. Buse, A. Adibi, and D. Psaltis, "Non-volatile holographic storage in doubly doped lithium niobate crystals," *Nature*, vol. 393, pp. 665–668, June 1998. doi: 10.1038/31429.
- [136] F. S. F. Chen, J. T. LaMacchia, and D. B. D. Fraser, "Holographic storage in lithium niobate," *Appl. Phys. Lett.*, vol. 13, no. 7, pp. 223–225, Oct. 1968. doi: 10.1063/1.1652580.
- [137] M. Carrascosa, A. García-Cabañes, M. Jubera, J. B. Ramiro, and F. Agulló-López, "LiNbO3: A photovoltaic substrate for massive parallel manipulation and patterning of nano-objects," *Appl. Phys. Rev.*, vol. 2, no. 4, p. 040605, Dec. 2015. doi: 10.1063/1.4929374.
- [138] N. Sinclair, D. Oblak, C. Thiel, R. Cone, and W. Tittel, "Properties of a rare-earth-ions-doped waveguide at sub-Kelvin temperatures for quantum signal processing," *Phys. Rev. Lett.*, vol. 118, no. 10, p. 100504, Mar. 2017. [Online]. Available: https://journals.aps.org/prl/abstract/10.1103/ PhysRevLett.118.100504
- [139] M. F. Askarani et al., Storage and retrieval of heralded telecommunication-wavelength photons using a solid-state waveguide quantum memory, arXiv:1804.05699, pp. 1–8, Apr. 2018.
- [140] P. Sharma et al., "Nonvolatile ferroelectric domain wall memory," *Sci. Adv.*, vol. 3, no. 6, pp. e1700512, 2017.
- [141] M. Schröder, A. Haußmann, A. Thiessen, E. Soergel, T. Woike, and L. M. Eng, "Conducting domain walls in lithium niobate single crystals," Adv. Funct. Mater., vol. 22, no. 18, pp. 3936–3944, Sept. 2012. doi: 10.1002/adfm.201201174.
- [142] K. Park, M. Esashi, and S. Tanaka, "Lithium-nio-bate-based surface acoustic wave device directly integrated on IC," in *Proc. 2011 IEEE Int. Ultrasonics Symp.*, pp. 1956–1959.